

An adaptive well-balanced positivity preserving central-upwind scheme on quadtree grids for shallow water equations

Mohammad A. Ghazizadeh^{a,*}, Abdolmajid Mohammadian^a, Alexander Kurganov^b

^a*Department of Civil Engineering, University of Ottawa, Ottawa, ON K1N 6N5, Canada*

^b*Department of Mathematics and SUSTech International Center for Mathematics, Southern University of Science and Technology, Shenzhen, 518055, China*

Abstract

We present an adaptive well-balanced positivity preserving central-upwind scheme on quadtree grids for shallow water equations. The use of quadtree grids results in a robust, efficient and highly accurate numerical method. The quadtree model is developed based on the well-balanced positivity preserving central-upwind scheme proposed in [A. KURGANOV AND G. PETROVA, *Commun. Math. Sci.*, 5 (2007), pp. 133–160]. The designed scheme is well-balanced in the sense that it is capable of exactly preserving “lake-at-rest” steady states. In order to achieve this as well as to preserve positivity of water depth, a continuous piecewise bilinear interpolation of the bottom topography function is utilized. This makes the proposed scheme capable of modelling flows over discontinuous bottom topography. Local gradients are examined to determine new seeding points in grid refinement for the next timestep. Numerical examples demonstrate the promising performance of the central-upwind quadtree scheme.

Keywords: Shallow water equations, quadtree grids, central-upwind scheme, well-balanced scheme, positivity preserving scheme.

1. Introduction

Quadtree grids (Figure 1), which are two-dimensional (2-D) semi-structured Cartesian grids, are based on hierarchical data structures, which are widely used in the field of computer science (e.g., image processing and computer graphics), computational geometry, robotics, video games, and computational fluid dynamics (CFD); see, e.g., [50, 57]. Several studies have been conducted on how to generate quadtree grids; see, e.g., [1, 12, 20, 42, 44, 49, 51].

Cartesian grids are common in CFD problems because of their efficiency and ability to maintain the simplicity of discretized equations, which reduces computational cost in comparison to unstructured grids. One of the benefits of quadtree grids over structured grids is grid coarsening: while the accuracy is maintained, the grid can be coarsened wherever no refinement is needed and thus, the computational cost is reduced. Note that a disadvantage of Cartesian grids is their inability to adequately represent complex shapes. In such situations, cut-cell grids become useful; see, e.g., [2]. This paper will only focus on quadtree grids.

*Corresponding author.

Email addresses: sghaz023@uottawa.ca (Mohammad A. Ghazizadeh), majid.mohammadian@uottawa.ca (Abdolmajid Mohammadian), alexander@sustech.edu.cn (Alexander Kurganov)

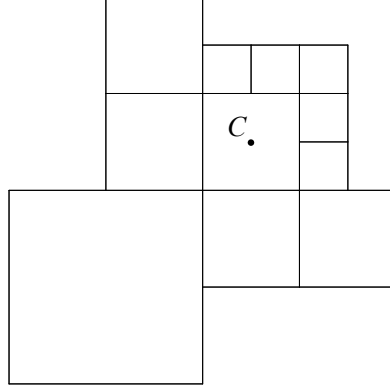


Figure 1: Example of quadtree cells with different level neighboring cell sizes.

The main goal of this paper is to develop an adaptive well-balanced positivity preserving scheme on quadtree grids for the Saint-Venant system of shallow water equations (SWEs). This system was first proposed in [15], but is still extensively used to model flows in rivers, lakes, coastal areas and estuaries [15]. In the 2-D case, the SWEs can be written in terms of the water surface (w) and the unit discharges (hu and hv) as follows [14]:

$$\begin{cases} w_t + (hu)_x + (hv)_y = 0, \\ (hu)_t + \left[\frac{(hu)^2}{w-B} + \frac{g}{2}(w-B)^2 \right]_x + \left[\frac{(hu)(hv)}{w-B} \right]_y = -g(w-B)B_x, \\ (hv)_t + \left[\frac{(hu)(hv)}{w-B} \right]_x + \left[\frac{(hv)^2}{w-B} + \frac{g}{2}(w-B)^2 \right]_y = -g(w-B)B_y, \end{cases} \quad (1.1)$$

where t is time, g is the gravitational constant, x and y are the directions in the 2-D Cartesian coordinate system, $u(x, y, t)$ and $v(x, y, t)$ are the water velocities in the x - and y -directions, respectively, $B(x, y)$ is the bottom topography, and $h(x, y, t) = w(x, y, t) - B(x, y)$ is the water depth.

The system (1.1) admits “lake-at-rest” steady-state solutions,

$$w \equiv \text{Const}, \quad u = v \equiv 0, \quad (1.2)$$

which are of great practical importance as many waves to be captured are, in fact, small perturbations of these steady states. We would like to stress that good numerical methods should be able of exactly preserving “lake-at-rest” steady states—such methods are called *well-balanced*. Another important property a good numerical method should possess is its ability to preserve non-negativity of water depth h —such methods are called *positivity preserving*. We refer the reader to, e.g., a recent review paper [23] for an extensive discussion on these matters.

Several numerical methods on quadtree grids for SWEs have been developed during the past two decades. For example, an adaptive well-balanced second-order Godunov-type scheme was proposed in [47]. This scheme is able to solve the shallow water system with discontinuous bottom topography. A well-balanced scheme on quadtree-cut-cell grids was proposed in [2]. This scheme is based on the hydrostatic reconstruction from [4]. In addition, an adaptive quadtree Roe-type scheme for the 2-D two-layer SWEs was introduced in [32]. Furthermore, an adaptive

quadtree scheme with wet-dry fronts was studied [34, 35]. For further studies on SWEs over quadtree grids, we refer the reader to [11, 12, 22, 36, 40]. Besides the aforementioned numerical methods, several well-balanced positivity preserving schemes have been proposed in the past years; see, e.g., [3, 4, 5, 8, 9, 10, 13, 17, 24, 27, 38, 45, 54], but none of them has been extended to quadtree grids.

In this paper, we present a central-upwind quadtree scheme which is based on the central-upwind scheme from [27]. Central-upwind schemes are Godunov-type Riemann-problem-solver-free finite-volume methods, which were proposed in [25, 26, 28, 29] as a “black-box” solvers for general multidimensional systems of hyperbolic systems of conservation laws. Central-upwind schemes were extended to shallow water models in [24] and many subsequent works; see, e.g., the recent review paper [23] and references therein. The scheme from [27] is the first well-balanced and at the same time positivity preserving central-upwind scheme, which is simple, efficient and robust: this is the reason why it was taken as the main building block of the proposed quadtree scheme.

The paper is organized as follows. In §2, we briefly describe a quadtree grid generation algorithm. In §3, we develop a well-balanced positivity preserving central-upwind quadtree scheme. The developed scheme is tested on three numerical example in §4. Finally, some concluding remarks can be found in §5.

2. Quadtree grids

Quadtree grids imply recursive spatial decomposition of the computational domain; see Figure 1 for an example of a quadtree cell C with different level neighboring cells.

Quadtree grids can be generated according to the following algorithm (see [12, 20]):

- Step 1.** Choose a domain and generate a set of seeding points considering features of the problem, boundary conditions, flow characteristics, local gradients and governing equations.
- Step 2.** Fit the domain within a unit square (root square) by adjusting the size of the square.
- Step 3.** Determine the level of refinement (m) of the quadtree (the size of the smallest cell of the grid is inversely proportional to m).
- Step 4.** Divide the domain square into four sub-squares. Each sub-square is called a cell (that is, the first level of the quadtree).
- Step 5.** Continue dividing each cell into four sub-cells if it contains a seeding point until the maximum refinement level is reached. If a cell does not include any seeding points, move to the next cell and again implement Step 5.

We note that in order to prevent complicated formulations and enhance the stability of the overall method, no cell can have both an adjacent neighboring cell and a diagonally neighboring cell with a refinement level difference greater than one; see [12, 20, 43]. This condition is satisfied provided the quadtree is regularized; several regularization algorithms can be found in [7, 41, 48, 52, 53, 56]. Examples of non-regularized and regularized quadtree grids are shown in Figure 2.

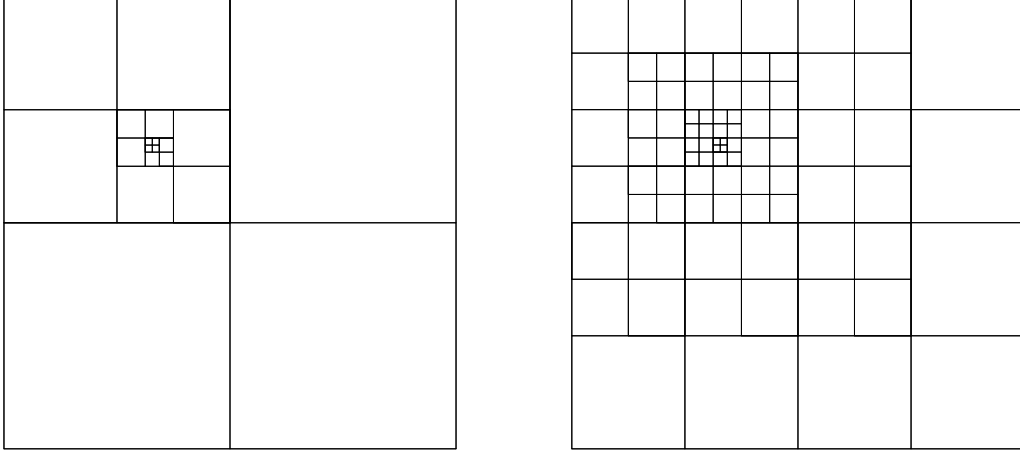


Figure 2: Examples of non-regularized (left) and regularized (right) quadtree grids.

3. Adaptive well-balanced semi-discrete central-upwind scheme

In this section, we present an adaptive well-balanced semi-discrete central-upwind scheme for the system (1.1), which can be written in the following vector form:

$$\mathbf{U}_t + \mathbf{F}(\mathbf{U}, B)_x + \mathbf{G}(\mathbf{U}, B)_y = \mathbf{S}(\mathbf{U}, B), \quad (3.1)$$

where

$$\mathbf{U} := (w, hu, hv)^\top,$$

and the fluxes and source term are:

$$\mathbf{F}(\mathbf{U}, B) = \left(hu, \frac{(hu)^2}{w - B} + \frac{g}{2}(w - B)^2, \frac{(hu)(hv)}{w - B} \right)^\top, \quad (3.2)$$

$$\mathbf{G}(\mathbf{U}, B) = \left(hv, \frac{(hu)(hv)}{w - B}, \frac{(hv)^2}{w - B} + \frac{g}{2}(w - B)^2 \right)^\top, \quad (3.3)$$

$$\mathbf{S}(\mathbf{U}, B) = (0, -g(w - B)B_x, -g(w - B)B_y)^\top. \quad (3.4)$$

The central-upwind quadtree scheme will be designed according to the following algorithm:

Step 1. Generate a non-regularized grid with the seeding points (§2).

Step 2. Regularize the non-regularized grid (§2).

Step 3. Perform piecewise polynomial reconstructions and obtain the required point values of the bottom topography B (§3.2) and conservative quantities \mathbf{U} (§3.3).

Step 4. Calculate the local speeds (§3.4) and central-upwind numerical fluxes (§3.5).

Step 5. Calculate the well-balanced discrete source term (§3.6).

Step 6. Calculate the size of timestep, which can guarantee the positivity and stability (§3.7).

Step 7. Calculate local gradients in each cell, which are needed to determine the seeding points at the next timestep (§3.8).

Step 8. Calculate current conservative quantities, which are going to be used as previous timestep data in the construction of the new quadtree grid (§3.8).

Step 9. Evolve the solution by solving the time-dependent system of ODEs, obtained after the semi-discretization of the studied SWEs over the quadtree grid.

3.1. Finite-volume semi-discretization over quadtree grids

Let us consider a typical finite-volume Cartesian cell $C_{j,k}$ of size $\Delta x_{j,k} \times \Delta y_{j,k}$ centered at $(x_{j,k}, y_{j,k})$. We assume that at a certain time level t , the computed solution is available and represented in terms of its cell averages:

$$\bar{\mathbf{U}}_{j,k}(t) \approx \frac{1}{\Delta x_{j,k} \Delta y_{j,k}} \int_{x_{j-\frac{1}{2}}}^{x_{j+\frac{1}{2}}} \int_{y_{k-\frac{1}{2}}}^{y_{k+\frac{1}{2}}} \mathbf{U}(x, y, t) dy dx, \quad (3.5)$$

where $x_{j\pm\frac{1}{2}} := x_{j,k} \pm \Delta x_{j,k}/2$ and $y_{k\pm\frac{1}{2}} := y_{j,k} \pm \Delta y_{j,k}/2$.

Considering the right and left neighbors of cell $C_{j,k}$, there exist nine different permutations of those neighboring cells; see Figure 3. We note, however, that only eight of them (configurations (a)–(h) in Figure 3) are possible in the proposed regularized quadtree grid. Similar cases are to be considered with respect to the neighboring cells on the top and bottom.

For the sake of brevity, we only present the quadtree scheme for configuration (b) in Figure 3 as an example of a quadtree cell (other configurations can be treated in a similar manner). We denote left-neighboring cells of $C_{j,k}$ by I and II . These two cells centered at $(x_{j,k} - 3\Delta x_{j,k}/4, y_{j,k} \pm \Delta y_{j,k}/4)$ are of size $\Delta x_{j,k}/2 \times \Delta y_{j,k}/2$.

The cell averages $\bar{\mathbf{U}}_{j,k}$ are evolved in time by solving the following system of time-dependent ODEs:

$$\frac{d}{dt} \bar{\mathbf{U}}_{j,k} = - \frac{\mathbf{H}_{j+\frac{1}{2},k}^x - \frac{\mathbf{H}_{j-\frac{1}{2},k-\frac{1}{4}}^x + \mathbf{H}_{j-\frac{1}{2},k+\frac{1}{4}}^x}{2}}{\Delta x_{j,k}} - \frac{\mathbf{H}_{j,k+\frac{1}{2}}^y - \mathbf{H}_{j,k-\frac{1}{2}}^y}{\Delta y_{j,k}} + \bar{\mathbf{S}}_{j,k}, \quad (3.6)$$

obtained after the semi-discretization of the system (3.1)–(3.4). In (3.6), $\mathbf{H}_{j+\frac{1}{2},k}^x$, $\mathbf{H}_{j-\frac{1}{2},k\pm\frac{1}{4}}^x$, $\mathbf{H}_{j,k+\frac{1}{2}}^y$ and $\mathbf{H}_{j,k-\frac{1}{2}}^y$ are the numerical fluxes, which, in general, are

$$\mathbf{H}_{\alpha,\beta}^x = \mathbf{H}^x(\mathbf{U}_{\alpha,\beta}^-, \mathbf{U}_{\alpha,\beta}^+; B_{\alpha,\beta}) \quad \text{and} \quad \mathbf{H}_{\gamma,\delta}^y = \mathbf{H}^y(\mathbf{U}_{\gamma,\delta}^-, \mathbf{U}_{\gamma,\delta}^+; B_{\gamma,\delta}) \quad (3.7)$$

where

$$\mathbf{U}_{\alpha,\beta}^\pm = \lim_{x \rightarrow x_\alpha \pm 0} \tilde{\mathbf{U}}(x, y_\beta) \quad \text{and} \quad \mathbf{U}_{\gamma,\delta}^\pm = \lim_{y \rightarrow y_\delta \pm 0} \tilde{\mathbf{U}}(x_\gamma, y), \quad (3.8)$$

and $\tilde{\mathbf{U}}$ is a piecewise polynomial interpolation. Second-order schemes employ piecewise linear interpolations,

$$\tilde{\mathbf{U}}(x, y) = (\mathbf{U}_x)_{j,k}[x - x_j] + (\mathbf{U}_y)_{j,k}[y - y_k], \quad (x, y) \in C_{j,k}, \quad (3.9)$$

where the slopes $(\mathbf{U}_x)_{j,k}$ and $(\mathbf{U}_y)_{j,k}$ are yet to be determined; see §3.3 below. Finally, $\bar{\mathbf{S}}_{j,k}$ is a cell average of the source term:

$$\bar{\mathbf{S}}_{j,k} \approx \frac{1}{\Delta x_{j,k} \Delta y_{j,k}} \int_{x_{j-\frac{1}{2}}}^{x_{j+\frac{1}{2}}} \int_{y_{k-\frac{1}{2}}}^{y_{k+\frac{1}{2}}} \mathbf{S}(\mathbf{U}, B) dy dx. \quad (3.10)$$

We note that all of the indexed quantities in (3.6)–(3.10) are time-dependent, but from now on we omit this dependence for the sake of brevity.

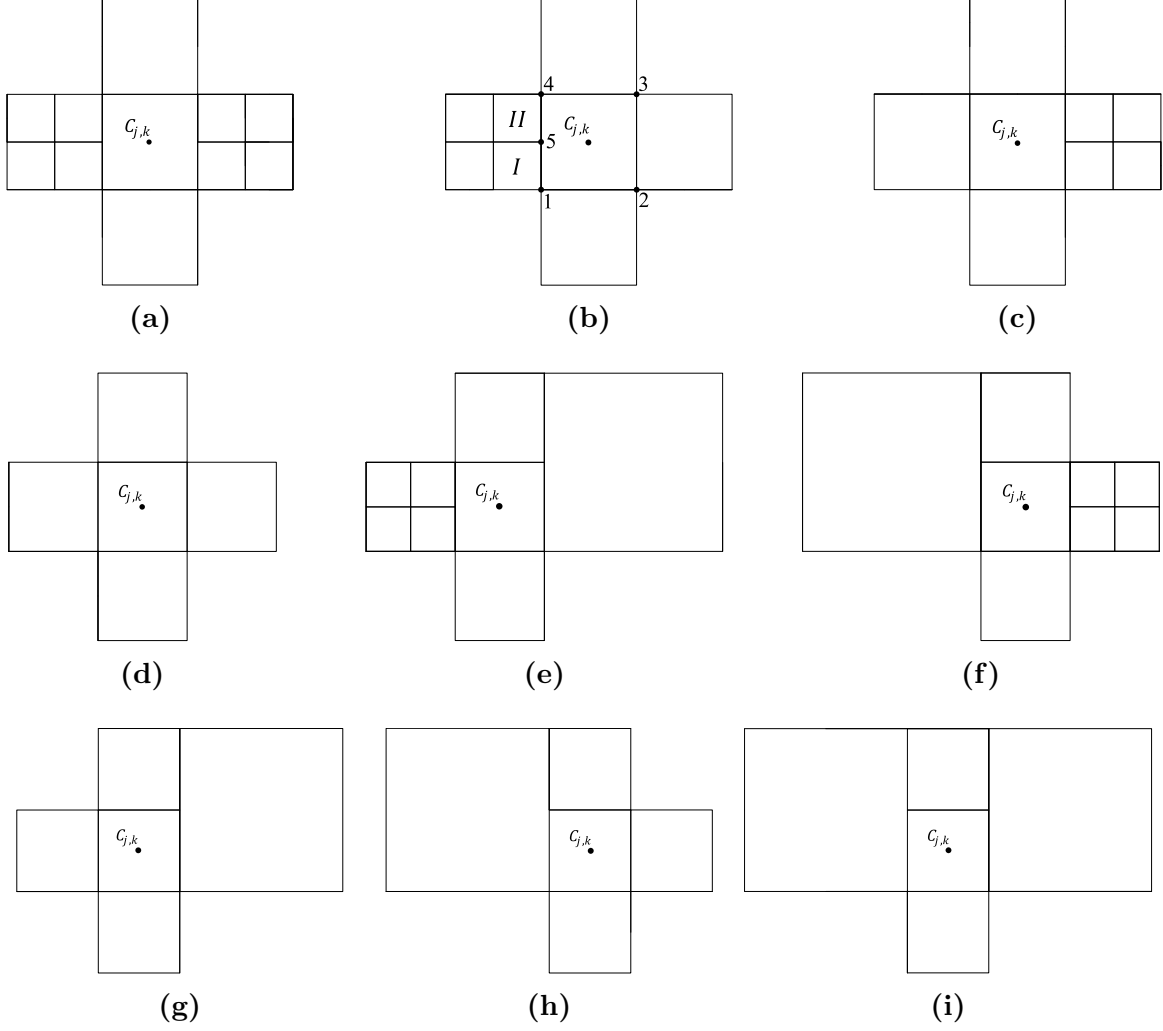


Figure 3: Permutations of neighboring cells of $C_{j,k}$ in the x -direction: (a)–(h) Possible configurations in regularized quadtree grids; (i) An impossible configuration in regularized quadtree grids.

3.2. Piecewise bilinear reconstruction of B

The quadtree grid consist of cells of different sizes: $\Delta x \times \Delta y, \frac{\Delta x}{2} \times \frac{\Delta y}{2}, \dots, \frac{\Delta x}{2^{m-1}} \times \frac{\Delta y}{2^{m-1}}$. We denote the set of cells of the corresponding size by $\mathcal{C}^{(\ell)}$, that is, $\mathcal{C}^{(\ell)} = \{C_{j,k} : |C_{j,k}| = \frac{\Delta x}{2^{\ell-1}} \times \frac{\Delta y}{2^{\ell-1}}\}$.

We follow the lines of [27] and use a continuous piecewise bilinear reconstruction of the bottom topography $\tilde{B}(x, y)$. We note that on a quadtree grid, the approach from [27] does not directly apply to a quadtree grid since it contains cells, whose vertex is a midpoint of the edge of the neighboring cell as point 5 in the configuration considered in Figure 3 (b). We therefore propose the following algorithm for constructing \tilde{B} .

Step 1. Set $\ell := 1$.

Step 2. Reconstruct bilinear pieces \tilde{B} for all (j, k) such that $C_{j,k} \in \mathcal{C}^{(\ell)}$. This is done as follows.

We first obtain the point values of B at the vertices of $C_{j,k}$. If one of them lies on the edge of a larger neighboring cell (which belongs to the set $\mathcal{C}^{(\ell-1)}$ where the bilinear piece has already been constructed), then there are two possibilities:

(i) either this vertex coincides with a vertex of the neighboring cell and then the point value of B has been already computed there;

(ii) or this vertex is a midpoint of the edge of the neighboring cell and then the point value of B at this vertex is an average of the point values of B at those two vertices of the neighboring cell that lie on the same edge (for example, in the configuration considered in Figure 3 (b), the value of B at point 5 will be equal to the average of the values of B at points 1 and 4).

Otherwise, we proceed as in [27] and set

$$B_{j\pm\frac{1}{2},k\pm\frac{1}{2}} := \frac{1}{2} \left(\max_{\xi^2+\eta^2=1} \lim_{\ell_x, \ell_y \rightarrow 0} B(x_{j\pm\frac{1}{2}} + \ell_x \xi, y_{k\pm\frac{1}{2}} + \ell_y \eta) + \min_{\xi^2+\eta^2=1} \lim_{\ell_x, \ell_y \rightarrow 0} B(x_{j\pm\frac{1}{2}} + \ell_x \xi, y_{k\pm\frac{1}{2}} + \ell_y \eta) \right),$$

which reduces to $B_{j\pm\frac{1}{2},k\pm\frac{1}{2}} = B(x_{j\pm\frac{1}{2}}, y_{k\pm\frac{1}{2}})$ if the function B is continuous at $(x_{j\pm\frac{1}{2}}, y_{k\pm\frac{1}{2}})$.

Equipped with the point values $B_{j\pm\frac{1}{2},k\pm\frac{1}{2}}$, we construct the following bilinear piece in cell $C_{j,k} \in \mathcal{C}^{(\ell)}$:

$$\begin{aligned} \tilde{B}(x, y) &= B_{j-\frac{1}{2},k-\frac{1}{2}} + (B_{j+\frac{1}{2},k-\frac{1}{2}} - B_{j-\frac{1}{2},k-\frac{1}{2}}) \frac{x - x_{j-\frac{1}{2}}}{\Delta x/2^{\ell-1}} + (B_{j-\frac{1}{2},k+\frac{1}{2}} - B_{j-\frac{1}{2},k-\frac{1}{2}}) \frac{y - y_{k-\frac{1}{2}}}{\Delta y/2^{\ell-1}} \\ &\quad + (B_{j+\frac{1}{2},k+\frac{1}{2}} - B_{j+\frac{1}{2},k-\frac{1}{2}} - B_{j-\frac{1}{2},k+\frac{1}{2}} + B_{j-\frac{1}{2},k-\frac{1}{2}}) \frac{x - x_{j-\frac{1}{2}}}{\Delta x/2^{\ell-1}} \cdot \frac{y - y_{k-\frac{1}{2}}}{\Delta y/2^{\ell-1}}, \quad (x, y) \in C_{j,k}. \end{aligned}$$

Step 3. Set $\ell := \ell + 1$.

Step 4. If $\ell \leq m$, then go to Step 2.

Note that the restriction of the interpolant \tilde{B} along each of the cell is a linear function and the cell average of \tilde{B} over the cell $C_{j,k}$ is equal to its value at the center of the cell and is also equal to the average of the values of \tilde{B} at the midpoints of the edges of $C_{j,k}$, namely, we have

$$B_{j,k} := \tilde{B}(x_j, y_k) = \frac{1}{\Delta x_{j,k} \Delta y_{j,k}} \iint_{C_{j,k}} \tilde{B}(x, y) dx dy = \frac{B_{j+\frac{1}{2},k} + B_{j-\frac{1}{2},k} + B_{j,k+\frac{1}{2}} + B_{j,k-\frac{1}{2}}}{4}, \quad (3.11)$$

where

$$B_{j\pm\frac{1}{2},k} := \tilde{B}(x_{j\pm\frac{1}{2}}, y_k) = \frac{1}{2} \left(B_{j\pm\frac{1}{2},k+\frac{1}{2}} + B_{j\pm\frac{1}{2},k-\frac{1}{2}} \right), \quad (3.12)$$

and

$$B_{j,k\pm\frac{1}{2}} := \tilde{B}(x_j, y_{k\pm\frac{1}{2}}) = \frac{1}{2} \left(B_{j+\frac{1}{2},k\pm\frac{1}{2}} + B_{j-\frac{1}{2},k\pm\frac{1}{2}} \right). \quad (3.13)$$

We also note that the values of B at the midpoints of the right edges of cells I and II in configuration considered in Figure 3 (b) can be obtained in a similar way:

$$B_{j-\frac{1}{2},k\pm\frac{1}{4}} := \tilde{B}(x_{j-\frac{1}{2}}, y_{k\pm\frac{1}{4}}) = \frac{1}{2} \left(B_{j-\frac{1}{2},k} + B_{j-\frac{1}{2},k\pm\frac{1}{2}} \right). \quad (3.14)$$

Formulae (3.11)–(3.14) are crucial for the proof of the positivity preserving property of our well-balanced quadtree central-upwind scheme; see §3.7.

Remark. We note that the proposed piecewise bilinear reconstruction can be applied to discontinuous bottom functions $B(x, y)$.

3.3. Piecewise linear reconstruction of \mathbf{U}

In this paper, we design a second-order scheme, which employs a piecewise linear reconstruction $\tilde{\mathbf{U}}$ in each cell. We then obtain the point values of \mathbf{U} (required in (3.7)) using (3.8), (3.9), which for cell $C_{j,k}$ from Figure 3 (b) results in

$$\begin{aligned} \mathbf{U}_{j+\frac{1}{2},k}^+ &= \bar{\mathbf{U}}_{j+1,k} - \frac{\Delta x_{j+1,k}}{2} (\mathbf{U}_x)_{j+1,k}, & \mathbf{U}_{j+\frac{1}{2},k}^- &= \bar{\mathbf{U}}_{j,k} + \frac{\Delta x_{j,k}}{2} (\mathbf{U}_x)_{j,k}, \\ \mathbf{U}_{j-\frac{1}{2},k\pm\frac{1}{4}}^+ &= \bar{\mathbf{U}}_{j,k} - \frac{\Delta x_{j,k}}{2} (\mathbf{U}_x)_{j,k} \pm \frac{\Delta y_{j,k}}{2} (\mathbf{U}_y)_{j,k}, \\ \mathbf{U}_{j-\frac{1}{2},k\pm\frac{1}{4}}^- &= \bar{\mathbf{U}}_{j-\frac{1}{4},k\pm\frac{1}{4}} + \frac{\Delta x_{j,k}}{4} (\mathbf{U}_x)_{j-\frac{1}{4},k\pm\frac{1}{4}} \end{aligned} \quad (3.15)$$

where $\bar{\mathbf{U}}_{j-\frac{1}{4},k-\frac{1}{4}}$ and $\bar{\mathbf{U}}_{j-\frac{1}{4},k+\frac{1}{4}}$ denote the cell averages of \mathbf{U} over the cells I and II , respectively.

In order to achieve the formal second order of accuracy, the slopes (\mathbf{U}_x) and (\mathbf{U}_y) in (3.15) are to be at least first-order approximations of the corresponding derivatives. In order to minimize oscillations, we compute the slopes using the minmod limiter (see, e.g., [6, 31, 55]), which is implemented in the following way:

$$\begin{aligned} (\mathbf{U}_x)_{j,k} &= \text{minmod} \left(\frac{\bar{\mathbf{U}}_{j,k} - \bar{\mathbf{U}}_{j-\frac{1}{4},k-\frac{1}{4}}}{3\Delta x_{j,k}/4}, \frac{\bar{\mathbf{U}}_{j,k} - \bar{\mathbf{U}}_{j-\frac{1}{4},k+\frac{1}{4}}}{3\Delta x_{j,k}/4}, \frac{\bar{\mathbf{U}}_{j+1,k} - \bar{\mathbf{U}}_{j,k}}{\Delta x_{j,k}} \right), \\ (\mathbf{U}_y)_{j,k} &= \text{minmod} \left(\frac{\bar{\mathbf{U}}_{j,k} - \bar{\mathbf{U}}_{j,k-1}}{\Delta y_{j,k}}, \frac{\bar{\mathbf{U}}_{j,k+1} - \bar{\mathbf{U}}_{j,k}}{\Delta y_{j,k}} \right) \end{aligned} \quad (3.16)$$

where the minmod function is defined by

$$\text{min}\{z_1, z_2, \dots\} := \begin{cases} \min_j \{z_j\}, & \text{if } z_j > 0 \quad \forall j, \\ \max_j \{z_j\}, & \text{if } z_j < 0 \quad \forall j, \\ 0, & \text{otherwise.} \end{cases}$$

3.3.1. Positivity preserving correction of w

The piecewise linear reconstruction (3.16) cannot guarantee the non-negativity of

$$\tilde{h}(x, y) := \tilde{w}(x, y) - \tilde{B}(x, y).$$

In fact, for the configuration considered in Figure 3 (b), we only need the following five inequalities to be satisfied:

$$\begin{aligned} h_{j-\frac{1}{2},k\pm\frac{1}{4}}^+ &= w_{j-\frac{1}{2},k\pm\frac{1}{4}}^+ - B_{j-\frac{1}{2},k\pm\frac{1}{4}} \geq 0, & h_{j+\frac{1}{2},k}^- &= w_{j+\frac{1}{2},k}^- - B_{j+\frac{1}{2},k} \geq 0, \\ h_{j,k-\frac{1}{2}}^+ &= w_{j,k-\frac{1}{2}}^+ - B_{j,k-\frac{1}{2}} \geq 0, & \text{and } h_{j,k+\frac{1}{2}}^- &= w_{j,k+\frac{1}{2}}^- - B_{j,k+\frac{1}{2}} \geq 0. \end{aligned}$$

If at least one of these inequalities is not satisfied, we need to correct \tilde{w} in the cell $C_{j,k}$. We note that the correction used in [27] will not in general work on quadtree grids. We therefore propose an alternative correction procedure and replace the linear pieces in the problematic cells with the bilinear one denoted by $\hat{w}(x, y)$ and constructed as follows. Let us denote by

$$\begin{aligned} w_{j,k}^{\text{NE}} &:= \tilde{w}(x_{j+\frac{1}{2}} - 0, y_{k+\frac{1}{2}} - 0), & w_{j,k}^{\text{SE}} &:= \tilde{w}(x_{j+\frac{1}{2}} - 0, y_{k-\frac{1}{2}} + 0), \\ w_{j,k}^{\text{NW}} &:= \tilde{w}(x_{j-\frac{1}{2}} + 0, y_{k+\frac{1}{2}} - 0), & w_{j,k}^{\text{SW}} &:= \tilde{w}(x_{j-\frac{1}{2}} + 0, y_{k-\frac{1}{2}} + 0) \end{aligned}$$

the four corner point values of the linear piece of \tilde{w} over the cell $C_{j,k}$. If

$$w_{j,k}^{\text{NE}} \geq B_{j+\frac{1}{2},k+\frac{1}{2}}, \quad w_{j,k}^{\text{SE}} \geq B_{j+\frac{1}{2},k-\frac{1}{2}}, \quad w_{j,k}^{\text{NW}} \geq B_{j-\frac{1}{2},k+\frac{1}{2}} \quad \text{and} \quad w_{j,k}^{\text{SW}} \geq B_{j-\frac{1}{2},k-\frac{1}{2}}, \quad (3.17)$$

then we set

$$\begin{aligned} \mathring{w}(x, y) = & w_{j,k}^{\text{SW}} + (w_{j,k}^{\text{SE}} - w_{j,k}^{\text{SW}}) \frac{x - x_{j-\frac{1}{2}}}{\Delta x_{j,k}} + (w_{j,k}^{\text{NW}} - w_{j,k}^{\text{SW}}) \frac{y - y_{k-\frac{1}{2}}}{\Delta y_{j,k}} \\ & + (w_{j,k}^{\text{NE}} - w_{j,k}^{\text{SE}} - w_{j,k}^{\text{NW}} + w_{j,k}^{\text{SW}}) \frac{x - x_{j-\frac{1}{2}}}{\Delta x_{j,k}} \cdot \frac{y - y_{k-\frac{1}{2}}}{\Delta y_{j,k}}, \quad (x, y) \in C_{j,k}. \end{aligned} \quad (3.18)$$

If at least one of the inequalities in (3.17) is not satisfied, we would first need to correct the point values of w at the vertices of $C_{j,k}$. There are three different cases to be considered.

Case 1: only one of the inequalities in (3.17) is not satisfied. Without loss of generality, we assume that $w_{j,k}^{\text{NE}} < B_{j+\frac{1}{2},k+\frac{1}{2}}$. We then replace the point values of w at the vertices of $C_{j,k}$ with

$$\begin{aligned} \mathring{w}_{j,k}^{\text{NE}} &= B_{j+\frac{1}{2},k+\frac{1}{2}}, \quad \mathring{w}_{j,k}^{\text{SE}} = B_{j+\frac{1}{2},k-\frac{1}{2}} + \frac{4}{3}(\bar{w}_{j,k} - B_{j,k}), \\ \mathring{w}_{j,k}^{\text{NW}} &= B_{j-\frac{1}{2},k+\frac{1}{2}} + \frac{4}{3}(\bar{w}_{j,k} - B_{j,k}), \quad \mathring{w}_{j,k}^{\text{SW}} = B_{j-\frac{1}{2},k-\frac{1}{2}} + \frac{4}{3}(\bar{w}_{j,k} - B_{j,k}). \end{aligned}$$

Case 2: only two of the inequalities in (3.17) are not satisfied. Without loss of generality, we assume that $w_{j,k}^{\text{NE}} < B_{j+\frac{1}{2},k+\frac{1}{2}}$ and $w_{j,k}^{\text{SE}} < B_{j+\frac{1}{2},k-\frac{1}{2}}$. We then replace the point values of w at the vertices of $C_{j,k}$ with

$$\begin{aligned} \mathring{w}_{j,k}^{\text{NE}} &= B_{j+\frac{1}{2},k+\frac{1}{2}}, \quad \mathring{w}_{j,k}^{\text{SE}} = B_{j+\frac{1}{2},k-\frac{1}{2}}, \\ \mathring{w}_{j,k}^{\text{NW}} &= B_{j-\frac{1}{2},k+\frac{1}{2}} + 2(\bar{w}_{j,k} - B_{j,k}), \quad \mathring{w}_{j,k}^{\text{SW}} = B_{j-\frac{1}{2},k-\frac{1}{2}} + 2(\bar{w}_{j,k} - B_{j,k}). \end{aligned}$$

Case 3: only three of the inequalities in (3.17) are not satisfied. Without loss of generality, we assume that $w_{j,k}^{\text{NE}} < B_{j+\frac{1}{2},k+\frac{1}{2}}$, $w_{j,k}^{\text{SE}} < B_{j+\frac{1}{2},k-\frac{1}{2}}$ and $w_{j,k}^{\text{NW}} < B_{j-\frac{1}{2},k+\frac{1}{2}}$. We then replace the point values of w at the vertices of $C_{j,k}$ with

$$\begin{aligned} \mathring{w}_{j,k}^{\text{NE}} &= B_{j+\frac{1}{2},k+\frac{1}{2}}, \quad \mathring{w}_{j,k}^{\text{SE}} = B_{j+\frac{1}{2},k-\frac{1}{2}}, \quad \mathring{w}_{j,k}^{\text{NW}} = B_{j-\frac{1}{2},k+\frac{1}{2}}, \\ \mathring{w}_{j,k}^{\text{SW}} &= 4\bar{w}_{j,k} - B_{j+\frac{1}{2},k+\frac{1}{2}} - B_{j+\frac{1}{2},k-\frac{1}{2}} - B_{j-\frac{1}{2},k+\frac{1}{2}}. \end{aligned}$$

In all of the above three cases, we use the corrected point values $\mathring{w}_{j,k}^{\text{NE}}$, $\mathring{w}_{j,k}^{\text{SE}}$, $\mathring{w}_{j,k}^{\text{NW}}$ and $\mathring{w}_{j,k}^{\text{SW}}$ to construct the corrected bilinear approximant (compare with (3.18))

$$\begin{aligned} \mathring{w}(x, y) = & \mathring{w}_{j,k}^{\text{SW}} + (\mathring{w}_{j,k}^{\text{SE}} - \mathring{w}_{j,k}^{\text{SW}}) \frac{x - x_{j-\frac{1}{2}}}{\Delta x_{j,k}} + (\mathring{w}_{j,k}^{\text{NW}} - \mathring{w}_{j,k}^{\text{SW}}) \frac{y - y_{k-\frac{1}{2}}}{\Delta y_{j,k}} \\ & + (\mathring{w}_{j,k}^{\text{NE}} - \mathring{w}_{j,k}^{\text{SE}} - \mathring{w}_{j,k}^{\text{NW}} + \mathring{w}_{j,k}^{\text{SW}}) \frac{x - x_{j-\frac{1}{2}}}{\Delta x_{j,k}} \cdot \frac{y - y_{k-\frac{1}{2}}}{\Delta y_{j,k}}, \quad (x, y) \in C_{j,k}. \end{aligned}$$

It is easy to show that the constructed bilinear piece $\mathring{w}(x, y)$ is conservative, that is,

$$\frac{1}{\Delta x_{j,k} \Delta y_{j,k}} \int_{C_{j,k}} \mathring{w}(x, y) \, dy \, dx = \bar{w}_{j,k},$$

and positivity preserving, that is,

$$\dot{w}(x, y) \geq \tilde{B}(x, y), \quad (x, y) \in C_{j,k}.$$

We also notice that the point values of w (required in (3.7)) at the cell $C_{j,k}$ from Figure 3 (b) are

$$\begin{aligned} w_{j-\frac{1}{2}, k \pm \frac{1}{4}}^+ &= \dot{w}(x_{j-\frac{1}{2}} + 0, y_{k \pm \frac{1}{4}}), & w_{j+\frac{1}{2}, k}^- &= \dot{w}(x_{j+\frac{1}{2}} - 0, y_k), \\ w_{j, k-\frac{1}{2}}^+ &= \dot{w}(x_j, y_{k-\frac{1}{2}} + 0), & w_{j, k+\frac{1}{2}}^- &= \dot{w}(x_j, y_{k+\frac{1}{2}} - 0) \end{aligned}$$

and thus the corresponding corrected values of h ,

$$\begin{aligned} h_{j-\frac{1}{2}, k \pm \frac{1}{4}}^+ &= w_{j-\frac{1}{2}, k \pm \frac{1}{4}}^+ - B_{j-\frac{1}{2}, k \pm \frac{1}{4}}, & h_{j+\frac{1}{2}, k}^- &= w_{j+\frac{1}{2}, k}^- - B_{j+\frac{1}{2}, k}, \\ h_{j, k-\frac{1}{2}}^+ &= w_{j, k-\frac{1}{2}}^+ - B_{j, k-\frac{1}{2}}, & h_{j, k+\frac{1}{2}}^- &= w_{j, k+\frac{1}{2}}^- - B_{j, k+\frac{1}{2}}, \end{aligned}$$

are nonnegative.

Finally, we would like to point out that the values of h at the boundaries of cell $C_{j,k}$ may be very small or even zero. This will require the computation of the corresponding point values of u and v to be desingularized. We use the desingularization approach from [27]:

$$u := \frac{\sqrt{2}h(hu)}{\sqrt{h^4 + \max\{h^4, \varepsilon\}}}, \quad v := \frac{\sqrt{2}h(hv)}{\sqrt{h^4 + \max\{h^4, \varepsilon\}}},$$

where we take $\varepsilon = \max\{\min_{j,k}\{(\Delta x_{j,k})^4\}, \min_{j,k}\{(\Delta y_{j,k})^4\}\}$. After recomputing the point values of h , u and v , the x - and y -discharges are also recalculated by setting:

$$(hu) := h \cdot u, \quad (hv) := h \cdot v.$$

Note that in the above two equations, we have omitted all of the indices for the sake of brevity.

3.4. Local speeds

The one-sided local speeds of propagation, denoted at the corresponding cell interfaces by $a_{\alpha,\beta}^\pm$ and $b_{\gamma,\delta}^\pm$, are calculated using the largest and smallest eigenvalues of the Jacobian matrices $\frac{\partial \mathbf{F}}{\partial \mathbf{U}}$ and $\frac{\partial \mathbf{G}}{\partial \mathbf{U}}$ and can be estimated by

$$\begin{aligned} a_{\alpha,\beta}^+ &= \max \left\{ u_{\alpha,\beta}^+ + \sqrt{gh_{\alpha,\beta}^+}, u_{\alpha,\beta}^- + \sqrt{gh_{\alpha,\beta}^-}, 0 \right\}, \\ a_{\alpha,\beta}^- &= \min \left\{ u_{\alpha,\beta}^+ - \sqrt{gh_{\alpha,\beta}^+}, u_{\alpha,\beta}^- - \sqrt{gh_{\alpha,\beta}^-}, 0 \right\}, \\ b_{\gamma,\delta}^+ &= \max \left\{ v_{\gamma,\delta}^+ + \sqrt{gh_{\gamma,\delta}^+}, v_{\gamma,\delta}^- + \sqrt{gh_{\gamma,\delta}^-}, 0 \right\}, \\ b_{\gamma,\delta}^- &= \min \left\{ v_{\gamma,\delta}^+ - \sqrt{gh_{\gamma,\delta}^+}, v_{\gamma,\delta}^- - \sqrt{gh_{\gamma,\delta}^-}, 0 \right\}. \end{aligned} \tag{3.19}$$

3.5. Central-upwind numerical fluxes

We use the central-upwind fluxes from [27], originally derived in [30]:

$$\begin{aligned}\mathbf{H}_{\alpha,\beta}^x &= \frac{a_{\alpha,\beta}^+ \mathbf{F}(\mathbf{U}_{\alpha,\beta}^-, B_{\alpha,\beta}) - a_{\alpha,\beta}^- \mathbf{F}(\mathbf{U}_{\alpha,\beta}^+, B_{\alpha,\beta})}{a_{\alpha,\beta}^+ - a_{\alpha,\beta}^-} + \frac{a_{\alpha,\beta}^+ a_{\alpha,\beta}^-}{a_{\alpha,\beta}^+ - a_{\alpha,\beta}^-} [\mathbf{U}_{\alpha,\beta}^+ - \mathbf{U}_{\alpha,\beta}^-], \\ \mathbf{H}_{\gamma,\delta}^y &= \frac{b_{\gamma,\delta}^+ \mathbf{G}(\mathbf{U}_{\gamma,\delta}^-, B_{\gamma,\delta}) - b_{\gamma,\delta}^- \mathbf{G}(\mathbf{U}_{\gamma,\delta}^+, B_{\gamma,\delta})}{b_{\gamma,\delta}^+ - b_{\gamma,\delta}^-} + \frac{b_{\gamma,\delta}^+ b_{\gamma,\delta}^-}{b_{\gamma,\delta}^+ - b_{\gamma,\delta}^-} [\mathbf{U}_{\gamma,\delta}^+ - \mathbf{U}_{\gamma,\delta}^-],\end{aligned}\tag{3.20}$$

where $(\alpha, \beta) \in \{(j - \frac{1}{2}, k - \frac{1}{4}), (j - \frac{1}{2}, k + \frac{1}{4}), (j + \frac{1}{2}, k)\}$ and $(\gamma, \delta) \in \{(j, k - \frac{1}{2}), (j, k + \frac{1}{2})\}$ in the configuration considered in Figure 3 (b).

3.6. Well-balanced discretization of the source term

A numerical scheme is well-balanced when the discretized cell average of the source term, $\bar{\mathbf{S}}_{j,k} = (0, \bar{S}_{j,k}^{(2)}, \bar{S}_{j,k}^{(3)})^\top$, exactly balances the numerical fluxes in equation (3.6) at the ‘‘lake-at-rest’’ steady state (1.2), that is, when the right-hand side (RHS) of (3.6) vanishes as long as $\bar{\mathbf{U}}_{j,k} \equiv (\hat{w}, 0, 0)^\top$ for all (j, k) , where \hat{w} is a constant.

We note that at the ‘‘lake-at-rest data’’, all of the reconstructed point values are $w^\pm = \tilde{w}$ and $u^\pm = v^\pm = 0$ and thus, $a_{\alpha,\beta}^+ = -a_{\alpha,\beta}^-$, $\forall(\alpha, \beta)$, $b_{\gamma,\delta}^+ = -b_{\gamma,\delta}^-$, $\forall(\gamma, \delta)$, and the numerical fluxes (3.20) reduce to

$$\mathbf{H}_{\alpha,\beta}^x = \left(0, \frac{g}{2} (\hat{w} - B_{\alpha,\beta})^2, 0\right)^\top, \quad \mathbf{H}_{\gamma,\delta}^y = \left(0, 0, \frac{g}{2} (\hat{w} - B_{\gamma,\delta})^2\right)^\top,$$

and the flux terms on the RHS of (3.6) then become

$$\begin{aligned}& - \frac{\mathbf{H}_{j+\frac{1}{2},k}^x - \frac{\mathbf{H}_{j-\frac{1}{2},k-\frac{1}{4}}^x + \mathbf{H}_{j-\frac{1}{2},k+\frac{1}{4}}^x}{2}}{\Delta x_{j,k}} - \frac{\mathbf{H}_{j,k+\frac{1}{2}}^y - \mathbf{H}_{j,k-\frac{1}{2}}^y}{\Delta y_{j,k}} \\ &= -\frac{g}{2} \left(\frac{\left(\hat{w} - B_{j+\frac{1}{2},k}\right)^2}{\Delta x_{j,k}} - \frac{\left(\hat{w} - B_{j-\frac{1}{2},k-\frac{1}{4}}\right)^2}{2\Delta x_{j,k}} - \frac{\left(\hat{w} - B_{j-\frac{1}{2},k+\frac{1}{4}}\right)^2}{2\Delta x_{j,k}} \right. \\ & \quad \left. - \frac{\left(\hat{w} - B_{j,k+\frac{1}{2}}\right)^2}{\Delta y_{j,k}} - \frac{\left(\hat{w} - B_{j,k-\frac{1}{2}}\right)^2}{\Delta y_{j,k}} \right).\end{aligned}\tag{3.21}$$

We now need to approximate the source term in (3.6) in such a way that $\bar{\mathbf{S}}_{j,k}$ would cancel (3.21) at the ‘‘lake-at-rest’’ steady states. To this end, we first notice that (at least for smooth solutions)

$$\begin{aligned}-g(w - B)B_x &= g(w - B)(w - B)_x - g(w - B)w_x = \frac{g}{2} [(w - B)^2]_x - g(w - B)w_x, \\ -g(w - B)B_y &= g(w - B)(w - B)_y - g(w - B)w_y = \frac{g}{2} [(w - B)^2]_y - g(w - B)w_y,\end{aligned}$$

and rewrite the cell averages of the second and third components of the integral in (3.10) as

$$\frac{g}{2} \int_{y_{k-\frac{1}{2}}}^{y_{k+\frac{1}{2}}} \left[(w - B)^2 \Big|_{x=x_{j+\frac{1}{2}}} - (w - B)^2 \Big|_{x=x_{j-\frac{1}{2}}} \right] dy - g \int_{x_{j-\frac{1}{2}}}^{x_{j+\frac{1}{2}}} \int_{y_{k-\frac{1}{2}}}^{y_{k+\frac{1}{2}}} (w - B)w_x dy dx\tag{3.22}$$

and

$$\frac{g}{2} \int_{x_{j-\frac{1}{2}}}^{x_{j+\frac{1}{2}}} \left[(w-B)^2 \Big|_{y=y_{k+\frac{1}{2}}} - (w-B)^2 \Big|_{y=y_{k-\frac{1}{2}}} \right] dx - g \int_{x_{j-\frac{1}{2}}}^{x_{j+\frac{1}{2}}} \int_{y_{k-\frac{1}{2}}}^{y_{k+\frac{1}{2}}} (w-B) w_y dy dx, \quad (3.23)$$

respectively. We then approximate the integrals in (3.22) and (3.23) using the second-order midpoint rule (for the configuration in Figure 3 (b), the integral along the left edge of $C_{j,k}$ is approximated using the composite midpoint rule as $C_{j,k}$ has two neighboring cells on the left), which results in the following quadrature for the second and third components of the source term:

$$\begin{aligned} \bar{S}_{j,k}^{(2)} \approx & \frac{g}{2\Delta x_{j,k}} \left[\left(w_{j+\frac{1}{2},k}^- - B_{j+\frac{1}{2},k} \right)^2 - \frac{\left(w_{j-\frac{1}{2},k-\frac{1}{4}}^+ - B_{j-\frac{1}{2},k-\frac{1}{4}} \right)^2}{2} \right. \\ & \left. - \frac{\left(w_{j-\frac{1}{2},k+\frac{1}{4}}^+ - B_{j-\frac{1}{2},k+\frac{1}{4}} \right)^2}{2} \right] - g(w_x)_{j,k} (\bar{w}_{j,k} - B_{j,k}), \end{aligned} \quad (3.24)$$

$$\bar{S}_{j,k}^{(3)} \approx \frac{g}{2\Delta y_{j,k}} \left[\left(w_{j,k+\frac{1}{2}}^- - B_{j,k+\frac{1}{2}} \right)^2 - \left(w_{j,k-\frac{1}{2}}^+ - B_{j,k-\frac{1}{2}} \right)^2 \right] - g(w_y)_{j,k} (\bar{w}_{j,k} - B_{j,k}).$$

We finally note that at the “lake-at-rest” data, $(w_x)_{j,k} = (w_y)_{j,k} \equiv 0$, $\forall(j,k)$ and thus (3.21) and (3.24) imply that the RHS of (3.6) vanishes and the resulting scheme is well-balanced.

3.7. Positivity preserving property and time discretization

One of the main advantages of the central-upwind scheme is its ability to preserve the positivity of h ; see [23, 27]. In this section, we extend the positivity proof from [27] to the proposed quadtree scheme. To this end, we integrate equation (3.6) in time using a forward Euler method. For the first component, this results in

$$\bar{w}_{j,k}^{n+1} = \bar{w}_{j,k}^n - \lambda_{j,k}^n \left(H_{j+\frac{1}{2},k}^{x,(1)} - \frac{H_{j-\frac{1}{2},k-\frac{1}{4}}^{x,(1)} + H_{j-\frac{1}{2},k+\frac{1}{4}}^{x,(1)}}{2} \right) - \mu_{j,k}^n \left(H_{j,k+\frac{1}{2}}^{y,(1)} - H_{j,k-\frac{1}{2}}^{y,(1)} \right), \quad (3.25)$$

where $\bar{w}_{j,k}^n := \bar{w}_{j,k}(t^n)$ and $\bar{w}_{j,k}^{n+1} := \bar{w}_{j,k}(t^{n+1})$ with $t^{n+1} = t^n + \Delta t^n$, $\lambda_{j,k}^n := \Delta t^n / \Delta x_{j,k}$, $\mu_{j,k}^n := \Delta t^n / \Delta y_{j,k}$, and the numerical fluxes on the RHS are evaluated at time level $t = t^n$ using (3.20):

$$\begin{aligned} H_{\alpha,\beta}^{x,(1)} &= \frac{a_{\alpha,\beta}^+(hu)_{\alpha,\beta}^- - a_{\alpha,\beta}^-(hu)_{\alpha,\beta}^+}{a_{\alpha,\beta}^+ - a_{\alpha,\beta}^-} + \frac{a_{\alpha,\beta}^+ a_{\alpha,\beta}^-}{a_{\alpha,\beta}^+ - a_{\alpha,\beta}^-} [w_{\alpha,\beta}^+ - w_{\alpha,\beta}^-], \\ H_{\gamma,\delta}^{y,(1)} &= \frac{b_{\gamma,\delta}^+(hv)_{\gamma,\delta}^- - b_{\gamma,\delta}^-(hv)_{\gamma,\delta}^+}{b_{\gamma,\delta}^+ - b_{\gamma,\delta}^-} + \frac{b_{\gamma,\delta}^+ b_{\gamma,\delta}^-}{b_{\gamma,\delta}^+ - b_{\gamma,\delta}^-} [w_{\gamma,\delta}^+ - w_{\gamma,\delta}^-], \end{aligned} \quad (3.26)$$

where, as before, $(\alpha, \beta) \in \{(j - \frac{1}{2}, k - \frac{1}{4}), (j - \frac{1}{2}, k + \frac{1}{4}), (j + \frac{1}{2}, k)\}$ and $(\gamma, \delta) \in \{(j, k - \frac{1}{2}), (j, k + \frac{1}{2})\}$ for the configuration considered in Figure 3 (b).

If $\bar{h}_{j,k}^n \geq 0$ for all (j, k) , then the point values of h computed using piecewise linear/bilinear reconstructions of w and B presented in §3.2 and §3.3, are nonnegative. Moreover, using (3.11)–(3.14) and the similar relationships for the reconstructed point values of w , we have

$$\bar{h}_{j,k}^n = \frac{1}{4} \left(\frac{h_{j-\frac{1}{2},k-\frac{1}{4}}^+ + h_{j-\frac{1}{2},k+\frac{1}{4}}^+}{2} + h_{j+\frac{1}{2},k}^- + h_{j,k-\frac{1}{2}}^+ + h_{j,k+\frac{1}{2}}^- \right) \quad (3.27)$$

for the configuration considered in Figure 3 (b).

We now subtract $B_{j,k}$ from both sides of (3.25) and use (3.26) and (3.27) to rewrite (3.25) as follows:

$$\begin{aligned} \bar{h}_{j,k}^{n+1} &= -\lambda_{j,k}^n a_{j+\frac{1}{2},k}^- \cdot \frac{a_{j+\frac{1}{2},k}^+ - u_{j+\frac{1}{2},k}^+}{a_{j+\frac{1}{2},k}^+ - a_{j+\frac{1}{2},k}^-} \cdot h_{j+\frac{1}{2},k}^+ + \left[\frac{1}{4} - \lambda_{j,k}^n a_{j+\frac{1}{2},k}^+ \cdot \frac{u_{j+\frac{1}{2},k}^- - a_{j+\frac{1}{2},k}^-}{a_{j+\frac{1}{2},k}^+ - a_{j+\frac{1}{2},k}^-} \right] h_{j+\frac{1}{2},k}^- \\ &+ \frac{\lambda_{j,k}^n a_{j-\frac{1}{2},k-\frac{1}{4}}^+}{2} \cdot \frac{u_{j-\frac{1}{2},k-\frac{1}{4}}^- - a_{j-\frac{1}{2},k-\frac{1}{4}}^-}{a_{j-\frac{1}{2},k-\frac{1}{4}}^+ - a_{j-\frac{1}{2},k-\frac{1}{4}}^-} \cdot h_{j-\frac{1}{2},k-\frac{1}{4}}^+ \\ &+ \frac{1}{2} \left[\frac{1}{4} - \lambda_{j,k}^n a_{j-\frac{1}{2},k-\frac{1}{4}}^- \cdot \frac{a_{j-\frac{1}{2},k-\frac{1}{4}}^+ - u_{j-\frac{1}{2},k-\frac{1}{4}}^+}{a_{j-\frac{1}{2},k-\frac{1}{4}}^+ - a_{j-\frac{1}{2},k-\frac{1}{4}}^-} \right] h_{j-\frac{1}{2},k-\frac{1}{4}}^+ \\ &+ \frac{\lambda_{j,k}^n a_{j-\frac{1}{2},k+\frac{1}{4}}^+}{2} \cdot \frac{u_{j-\frac{1}{2},k+\frac{1}{4}}^- - a_{j-\frac{1}{2},k+\frac{1}{4}}^-}{a_{j-\frac{1}{2},k+\frac{1}{4}}^+ - a_{j-\frac{1}{2},k+\frac{1}{4}}^-} \cdot h_{j-\frac{1}{2},k+\frac{1}{4}}^+ \\ &+ \frac{1}{2} \left[\frac{1}{4} - \lambda_{j,k}^n a_{j-\frac{1}{2},k+\frac{1}{4}}^- \cdot \frac{a_{j-\frac{1}{2},k+\frac{1}{4}}^+ - u_{j-\frac{1}{2},k+\frac{1}{4}}^+}{a_{j-\frac{1}{2},k+\frac{1}{4}}^+ - a_{j-\frac{1}{2},k+\frac{1}{4}}^-} \right] h_{j-\frac{1}{2},k+\frac{1}{4}}^+ \\ &- \mu_{j,k}^n b_{j,k+\frac{1}{2}}^- \cdot \frac{b_{j,k+\frac{1}{2}}^+ - v_{j,k+\frac{1}{2}}^+}{b_{j,k+\frac{1}{2}}^+ - b_{j,k+\frac{1}{2}}^-} \cdot h_{j,k+\frac{1}{2}}^+ + \left[\frac{1}{4} - \mu_{j,k}^n b_{j,k+\frac{1}{2}}^+ \cdot \frac{v_{j,k+\frac{1}{2}}^- - b_{j,k+\frac{1}{2}}^-}{b_{j,k+\frac{1}{2}}^+ - b_{j,k+\frac{1}{2}}^-} \right] h_{j,k+\frac{1}{2}}^- \\ &+ \mu_{j,k}^n b_{j,k-\frac{1}{2}}^+ \cdot \frac{v_{j,k-\frac{1}{2}}^- - b_{j,k-\frac{1}{2}}^-}{b_{j,k-\frac{1}{2}}^+ - b_{j,k-\frac{1}{2}}^-} \cdot h_{j,k-\frac{1}{2}}^- + \left[\frac{1}{4} + \mu_{j,k}^n b_{j,k-\frac{1}{2}}^- \cdot \frac{b_{j,k-\frac{1}{2}}^+ - v_{j,k-\frac{1}{2}}^+}{b_{j,k-\frac{1}{2}}^+ - b_{j,k-\frac{1}{2}}^-} \right] h_{j,k-\frac{1}{2}}^+ \end{aligned}$$

This shows that the cell averages of h at the new time level can be written as a linear combination of the reconstructed nonnegative point values of h . Therefore, $\bar{h}_{j,k}^{n+1} \geq 0$ provided all of the coefficients in this linear combination are nonnegative, which is, using the definition of the local speeds of propagation in (3.19), true provided the following CFL-type condition are satisfied:

$$\Delta t \leq \frac{1}{4} \min \left[\min_{j,k} \left\{ \frac{\Delta x_{j,k}}{\max_{(\alpha,\beta)} [\max \{a_{\alpha,\beta}^+, -a_{\alpha,\beta}^- \}]} \right\}, \min_{j,k} \left\{ \frac{\Delta y_{j,k}}{\max_{(\gamma,\delta)} [\max \{b_{\gamma,\delta}^+, -b_{\gamma,\delta}^- \}]} \right\} \right].$$

where, as before, $(\alpha, \beta) \in \{(j - \frac{1}{2}, k - \frac{1}{4}), (j - \frac{1}{2}, k + \frac{1}{4}), (j + \frac{1}{2}, k)\}$ and $(\gamma, \delta) \in \{(j, k - \frac{1}{2}), (j, k + \frac{1}{2})\}$ for the configuration considered in Figure 3 (b).

It should be observed that the above positivity preserving proof is valid not only for the forward Euler time discretization, but for any strong stability preserving (SSP) ODE solver (see, e.g., [18, 19]) as well. In all of our numerical experiments, we have used the three-stage third-order SSP Runge-Kutta solver.

3.8. Quadtree grid adaptivity

After evolving the solution to the new time level $t = t^{n+1}$ the quadtree grid should be adapted (locally either refined or coarsened) to the new solution structure. To this end, we first compute the slopes $\{(w_x)_{j,k}^{n+1}\}$ and $\{(w_y)_{j,k}^{n+1}\}$ on the old grid (which we denote by $\{C_{j,k}^{\text{old}}\}$) according to §3.3 and then select the centers of those cells $C_{j,k}^{\text{old}}$, at which either

$$(w_x)_{j,k}^{n+1} \geq C_{\text{seed}} \quad \text{or} \quad (w_y)_{j,k}^{n+1} \geq C_{\text{seed}}, \quad (3.28)$$

to be the seeding points needed to generate the new grid, which we denote by $\{C_{j,k}^{\text{new}}\}$. In (3.28), C_{seed} is a constant that depends on the problem at hand, that is, on such factors as the Froude number, bottom topography function and/or boundary conditions.

When the mesh is locally refined or coarsened, the solution realized at the end of the evolution step in terms of the computed cell averages $\{(\bar{\mathbf{U}}_{j,k}^{n+1})_{\text{old}}\}$ over the grid $\{C_{j,k}^{\text{old}}\}$, should be projected onto the new grid $\{C_{j,k}^{\text{new}}\}$ in a conservative manner according to the following three possible cases.

Case 1: If $C_{j,k}^{\text{new}} = C_{j',k'}^{\text{old}}$ for some (j', k') , that is, if the cell $C_{j',k'}^{\text{old}}$ does not need to be refined/coarsened, then

$$(\bar{\mathbf{U}}_{j,k}^{n+1})_{\text{new}} = (\bar{\mathbf{U}}_{j',k'}^{n+1})_{\text{old}}.$$

Case 2: If $C_{j,k}^{\text{new}} \in \mathcal{C}^{\ell+p}$ is a ‘‘child’’ cell of $C_{j',k'}^{\text{old}} \in \mathcal{C}^{\ell}$ for some j', k' and $p > 0$ (that is, if the cell $C_{j',k'}^{\text{old}}$ was refined and $C_{j,k}^{\text{new}} \subset C_{j',k'}^{\text{old}}$), then

$$(\bar{\mathbf{U}}_{j,k}^{n+1})_{\text{new}} = (\bar{\mathbf{U}}_{j',k'}^{n+1})_{\text{old}} + ((\mathbf{U}_x)_{j',k'}^{n+1})_{\text{old}} [x_j^{\text{new}} - x_{j'}^{\text{old}}] + ((\mathbf{U}_y)_{j',k'}^{n+1})_{\text{old}} [y_k^{\text{new}} - y_{k'}^{\text{old}}].$$

Case 3: If $C_{j,k}^{\text{new}} \in \mathcal{C}^{\ell-p}$ is a ‘‘parent’’ cell of $C_{j',k'}^{\text{old}} \in \mathcal{C}^{\ell}$ for some j', k' and $p > 0$ (that is, if the cell $C_{j',k'}^{\text{old}}$ was coarsened and $C_{j,k}^{\text{new}} \supset C_{j',k'}^{\text{old}}$), then

$$(\bar{\mathbf{U}}_{j,k}^{n+1})_{\text{new}} = \frac{1}{4^p} \sum_{j'', k'': C_{j'', k''}^{\text{old}} \subset C_{j,k}^{\text{new}}} (\bar{\mathbf{U}}_{j'', k''}^{n+1})_{\text{old}}.$$

4. Numerical experiments

In this section, we present six numerical examples in which the central-upwind quadtree scheme is tested. In all of the examples (except for Example 5), we take $g = 1$ and obtain the point values of B at the vertices of $C_{j,k}$ using the bottom topography function with $\ell := 5$ (§3.2).

Example 1 — Accuracy test

In this benchmark, the accuracy of the proposed scheme is tested. We set the computational domain $[0, 2] \times [0, 1]$ with a zero-order extrapolation at all of the boundaries. The following initial data and the bottom topography function are imposed:

$$w(x, y, 0) \equiv 1, \quad u(x, y, 0) \equiv 0.3, \quad v(x, y, 0) \equiv 0, \quad B(x, y) = 0.5e^{-25(x-1)^2 - 50(y-0.5)^2}.$$

We generate a structured Cartesian grid $[512 \times 256]$ for the reference solution. The solution converges to a steady state solution by $t = 0.07$. The L^1 - and L^∞ -errors for $m = 5, 6, 7$, and 8 for $C_{\text{seed}} = 0.0005$ are presented in Table 1. The obtained errors are similar to the ones reported in [13, 27, 54]. The steady state solution computed with $m = 7$ and the corresponding quadtree grid are shown in Figure 4.

Table 1: Example 1: L^1 - and L^∞ - errors and numerical orders of accuracy.

Quadtree level	L^1 -error	Order	L^∞ -error	Order
$m = 5$	$8.97e - 04$	—	$5.14e - 03$	—
$m = 6$	$4.35e - 04$	1.05	$3.22e - 03$	0.67
$m = 7$	$2.80e - 04$	1.68	$2.90e - 03$	0.83
$m = 8$	$2.32e - 04$	1.95	$2.18e - 03$	1.24

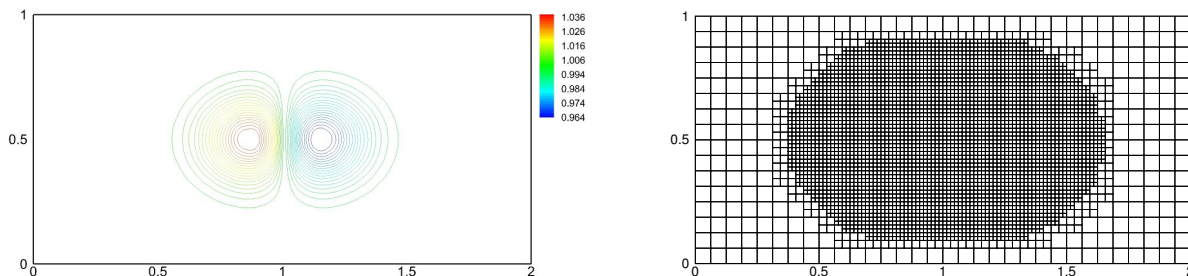


Figure 4: Example 1: Computed water surface $w(x, y, 0.07)$ for $m = 7$ (left) and its corresponding quadtree grid (right).

Example 2 — Circular dam break

In this example, we demonstrate the ability of the proposed central-upwind quadtree scheme to preserve the positivity of the water surface and to maintain symmetry. A circular water column, where $w = 1$, collapses on a horizontal plane (similar examples were considered in [4, 37, 47, 46]), namely,

$$w(x, y, 0) = \begin{cases} 1, & (x - 1)^2 + (y - 1)^2 < 0.25, \\ 10^{-16}, & \text{otherwise,} \end{cases} \quad u(x, y, 0) = v(x, y, 0) \equiv 0.$$

We take the computational domain $[0, 2] \times [0, 2]$ and impose zero-order extrapolated boundary conditions at its boundary. In this example, we take $m = 8$ and $m = 9$ refinement levels of the quadtree grid and set $C_{\text{seed}} = 0.1$ in (3.28). The initial quadtree grids are shown in Figure 5.

We compute the solution until the final time $t = 0.2$ and plot the obtained water surface contours in Figure 6. As one can see, the central-upwind quadtree scheme maintains symmetry and preserves positivity. By changing the refinement level from $m = 8$ to $m = 9$, the computational cost increases (for $m = 8$, the quadtree grid starts with 1852 cells and ends with 12556 cells, whereas for $m = 9$, the grid starts with 3616 cells and ends with 56272 cells), but the results obtained with $m = 9$ are clearly sharper and more accurate.

Example 3 — Small perturbations of a stationary steady-state solution

This numerical example is based on the benchmark, which was proposed in [33] to test the ability of studied schemes to accurately capture small perturbations of a steady state solution (similar examples were considered in, e.g., [13, 14, 24, 39, 54]). The computational domain is $[0, 2] \times [0, 1]$, the initial conditions are

$$w(x, y, 0) = \begin{cases} 1 + \varepsilon, & 0.05 < x < 0.15, \\ 1, & \text{otherwise,} \end{cases} \quad u(x, y, 0) = v(x, y, 0) \equiv 0,$$

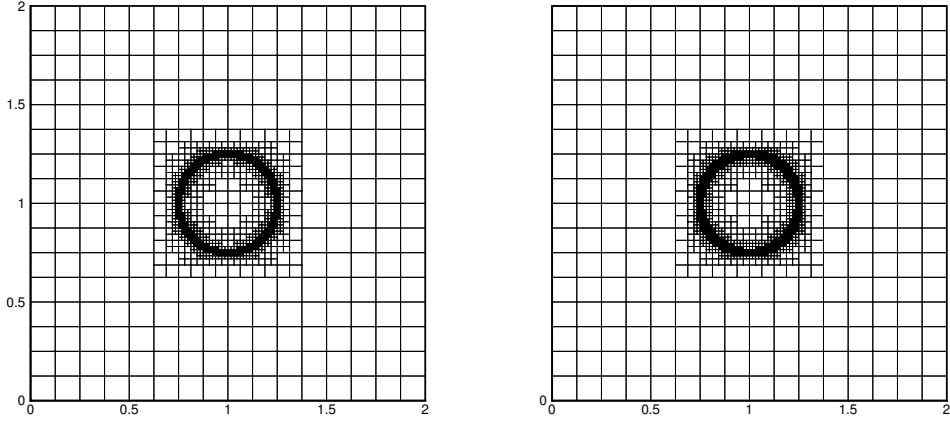


Figure 5: Example 2: Initial quadtree grids for $m = 8$ (left) and $m = 9$ (right).

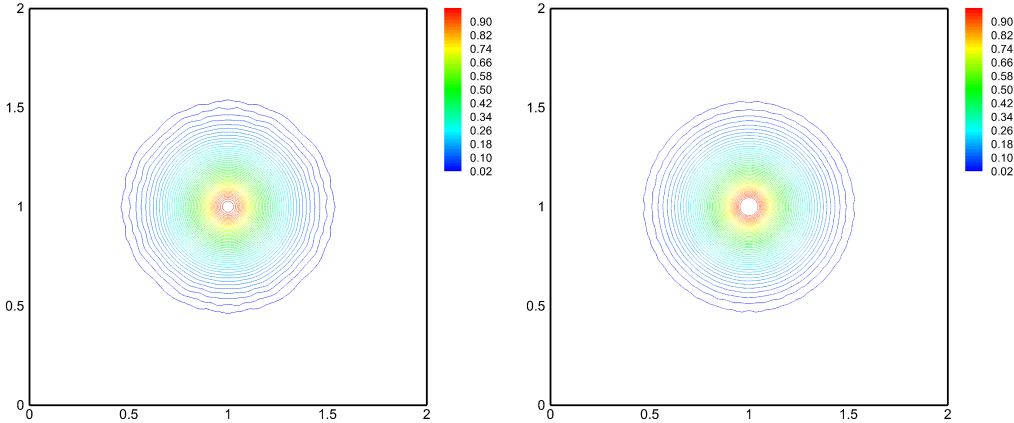


Figure 6: Example 2: Computed water surface $w(x, y, 0.2)$ for $m = 8$ (left) and $m = 9$ (right).

and the bottom topography is given by

$$B(x, y) = 0.8e^{-5(x-0.9)^2-50(y-0.5)^2}.$$

A solid wall boundary condition is used at the top and bottom boundaries and zero-order extrapolation is implemented at the left and right ones. We first consider a very small value $\varepsilon = 10^{-14}$ to verify the well-balanced property of the proposed quadtree scheme. The solution is solved with a coarse quadtree grid for $m = 5$. In Figure 7, we plot $\max_{x,y}(w - 1)$ as a function of time until $t = 0.6$. As one can see, the proposed scheme is stable and the fluxes and source terms balance each other.

We then take $\varepsilon = 0.01$ and $m = 8$ refinement levels of the quadtree grid and set small $C_{\text{seed}} = 0.02$ in (3.28) in order to accurately resolve small features of the computed solution. We compute the solution until the final time $t = 1.8$ and plot the snapshots of w at times $t = 0.6, 0.9, 1.2, 1.5$ and 1.8 in Figure 8 (left). The quadtree grid starts with 1970 cells and reaches a maximum number of 7268 cells during the time evolution. Figure 8 (left) clearly demonstrate that the proposed well-balanced central-upwind quadtree scheme accurately captures a small

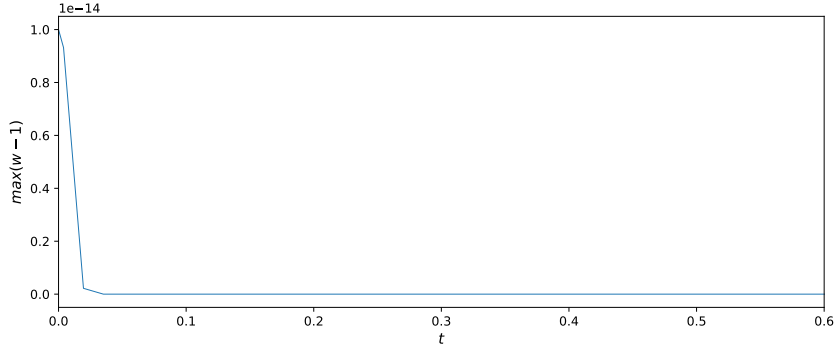


Figure 7: Example 2: Computed $\max_{x,y} w(x, y, t)$ as a function of t for $m = 5$.

perturbation of the “lake-at-rest” steady state and that the symmetry of the solution is preserved. The ability of the scheme to refine grids where local gradients are sharp can be seen in Figure 8 (right), where the quadtree grids at the same times $t = 0.6, 0.9, 1.2, 1.5$ and 1.8 are presented.

We also solve this initial-boundary value problem using a non-well-balanced central-upwind quadtree scheme to stress the importance of the well-balanced property. In order to design a non-well-balanced scheme, we replace the well-balanced numerical source terms $\bar{S}_{j,k}^{(2)}$ and $\bar{S}_{j,k}^{(3)}$ given by (3.24) with the source terms obtained by a straightforward midpoint rule quadrature. For the configuration considered in Figure 3 (b), the non-well-balanced source term approximations read as

$$\begin{aligned} \bar{S}_{j,k}^{(2)} &= -\frac{g(\bar{w}_{j,k} - B_{j,k})}{\Delta x_{j,k}} \left[\frac{B_{j+\frac{1}{2},k+\frac{1}{2}} + B_{j+\frac{1}{2},k-\frac{1}{2}}}{2} - \frac{B_{j-\frac{1}{2},k+\frac{1}{2}} + B_{j-\frac{1}{2},k-\frac{1}{2}}}{2} \right], \\ \bar{S}_{j,k}^{(3)} &= -\frac{g(\bar{w}_{j,k} - B_{j,k})}{\Delta x_{j,k}} \left[\frac{B_{j+\frac{1}{2},k+\frac{1}{2}} + B_{j+\frac{1}{2},k-\frac{1}{2}}}{2} - \frac{B_{j-\frac{1}{2},k+\frac{1}{2}} + B_{j-\frac{1}{2},k-\frac{1}{2}}}{2} \right]. \end{aligned}$$

Figure 9 shows the snapshots of w at times $t = 0.6, 0.9, 1.2, 1.5$ and 1.8 and the corresponding quadtree grids obtained using the non-well-balanced computations. As one can see, the use of non-well-balanced numerical source term leads to the appearance of not small “parasitic” waves. Even though these waves are not as large as in the non-well-balanced results presented in, e.g., [13] or [39], the unphysical oscillations caused by the non-well-balanced discretization of the source term are attenuated by adding more seeding points as the quadtree grid reaches a maximum number of 8900 cells during the time evolution. This demonstrates the importance of the well-balanced property, which eventually reduces the computational cost.

Example 4 — Small perturbations over a submerged flat plateau

In this example, which is similar to the examples considered in [13, 54], we study small perturbations over a submerged flat plateau. The computational domain is $[0, 1] \times [0, 1]$. A solid wall boundary condition is used at the top and bottom boundaries and zero-order extrapolation

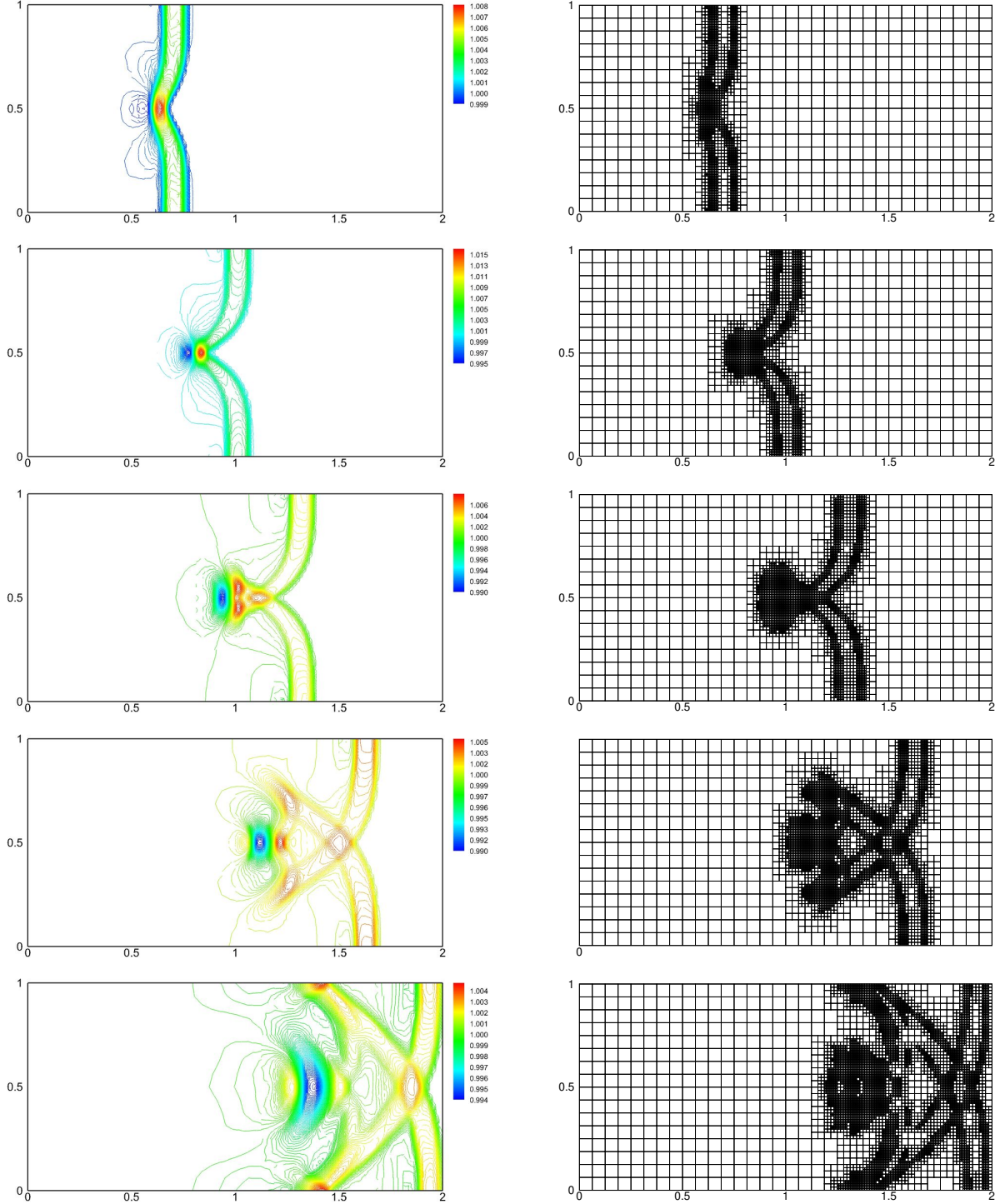


Figure 8: Example 3: Computed water surface $w(x, y, t)$ (left column) and the corresponding quadtree grids (right column) for $t = 0.6, 0.9, 1.2, 1.5$ and 1.8 (from top to down) obtained using the well-balanced central-upwind quadtree scheme.

is implemented at the left and right ones. The bottom topography function is given by

$$B(x, y) = \begin{cases} 1 - 2\varepsilon, & r \leq 0.1, \\ 10(1 - 2\varepsilon)(0.2 - r), & 0.1 \leq r \leq 0.2, \\ 0, & \text{otherwise,} \end{cases}$$

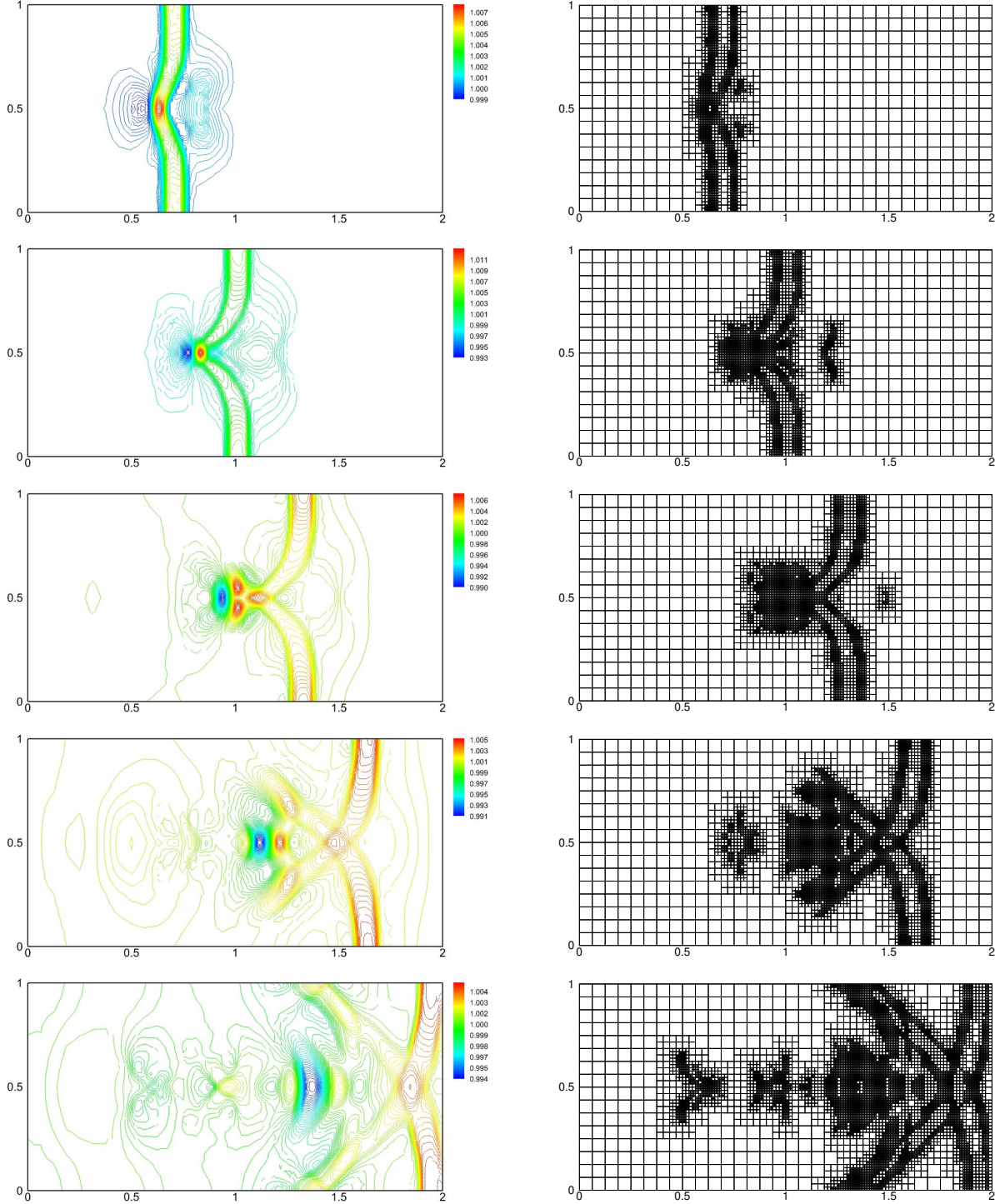


Figure 9: Same as Figure 8, but for the non-well-balanced central-upwind quadtree scheme.

where $\varepsilon = 10^{-4}$ and $r = \sqrt{(x - 0.5)^2 + (y - 0.5)^2}$. The following initial data are imposed:

$$w(x, y, 0) = \begin{cases} 1 + \varepsilon, & 0.1 \leq x \leq 0.2, \\ 1, & \text{otherwise,} \end{cases} \quad u(x, y, 0) = v(x, y, 0) \equiv 0.$$

We compute both well-balanced and non-well-balanced solutions with $m = 8$ and $C_{\text{seed}} = 0.0002$. The obtained w (left column) and the corresponding quadtree grids (right column) at $t = 0.2, 0.35, 0.5$, and 0.65 are shown in Figures 10 and 11. We note that the number of cells in the well-balanced computation varies from 3712 to 13384, while in the non-well-balanced one it goes up to a much larger maximum of 34126 cells. However, this level of refinement is apparently not enough to suppress the non-physical parasitic waves, which propagate all over the computational domain; see Figure 11. On the contrary, the well-balanced solution is oscillation-free as one can clearly see in Figure 10.

Example 5 — Cylindrical dam break over a step

In this example taken from [16], we demonstrate the capability of the proposed scheme to solve problems with discontinuous bottom topography. We consider the following initial conditions and bottom topography:

$$h(x, y, 0) = \begin{cases} 1, & r \leq 1, \\ 0.5, & r > 1, \end{cases} \quad u(x, y, 0) = v(x, y, 0) \equiv 0, \quad B(x, y) = \begin{cases} -0.2, & r \leq 1, \\ 0, & r > 1, \end{cases}$$

where $r = \sqrt{(x-2)^2 + (y-2)^2}$. The computational domain is $[0, 4] \times [0, 4]$, $g = 9.8$ and the point values of B at the vertices of $C_{j,k}$ are obtained using the bottom topography function with $\ell := 6$ (§3.2). We compute the solution until the final time $t = 0.2$ using $C_{\text{seed}} = 0.1$ and $m = 8$. Figure 12 shows the obtained w at times $t = 0.05, 0.1, 0.15$ and 0.2 , and the corresponding quadtree grids. The number of cells at time $t = 0$ is 6172 and it reaches a maximum of 12508 cells at later times. As one can see, the proposed scheme is capable of accurately capturing the solution in the case of discontinuous bottom topography.

Example 6 — Sudden contraction

The last example is a modification of the benchmark in [21]; also see [14, 13]. The purpose of this example is twofold: to show the ability of the central-upwind quadtree scheme to capture shocks and sharp waves in supercritical flows and to demonstrate the positivity preserving property of the proposed scheme.

We consider an open channel with a sudden contraction. The geometry of the channel is established on its contraction, where

$$y_b(x) = \begin{cases} 0.5, & x \leq 1, \\ 0.4, & \text{otherwise.} \end{cases}$$

The computational domain is $[0, 3] \times [0.5 - y_b(x), 0.5 + y_b(x)]$. Solid wall boundary conditions are imposed at all of the boundaries except for the left (inflow boundary with $u(0, y, t) \equiv 2$) and right (zero-order extrapolation) ones. The following initial conditions are prescribed:

$$w(x, y, 0) \equiv 1, \quad u(x, y, 0) \equiv 2, \quad v(x, y, 0) \equiv 0.$$

In this example, we take $m = 8$ and $m = 9$ refinement levels of the quadtree grid and set $C_{\text{seed}} = 2$ in (3.28). This value of C_{seed} is greater than the ones used in Examples 1 and 2 since this numerical experiment focuses on capturing sharp waves and thus choosing small values of

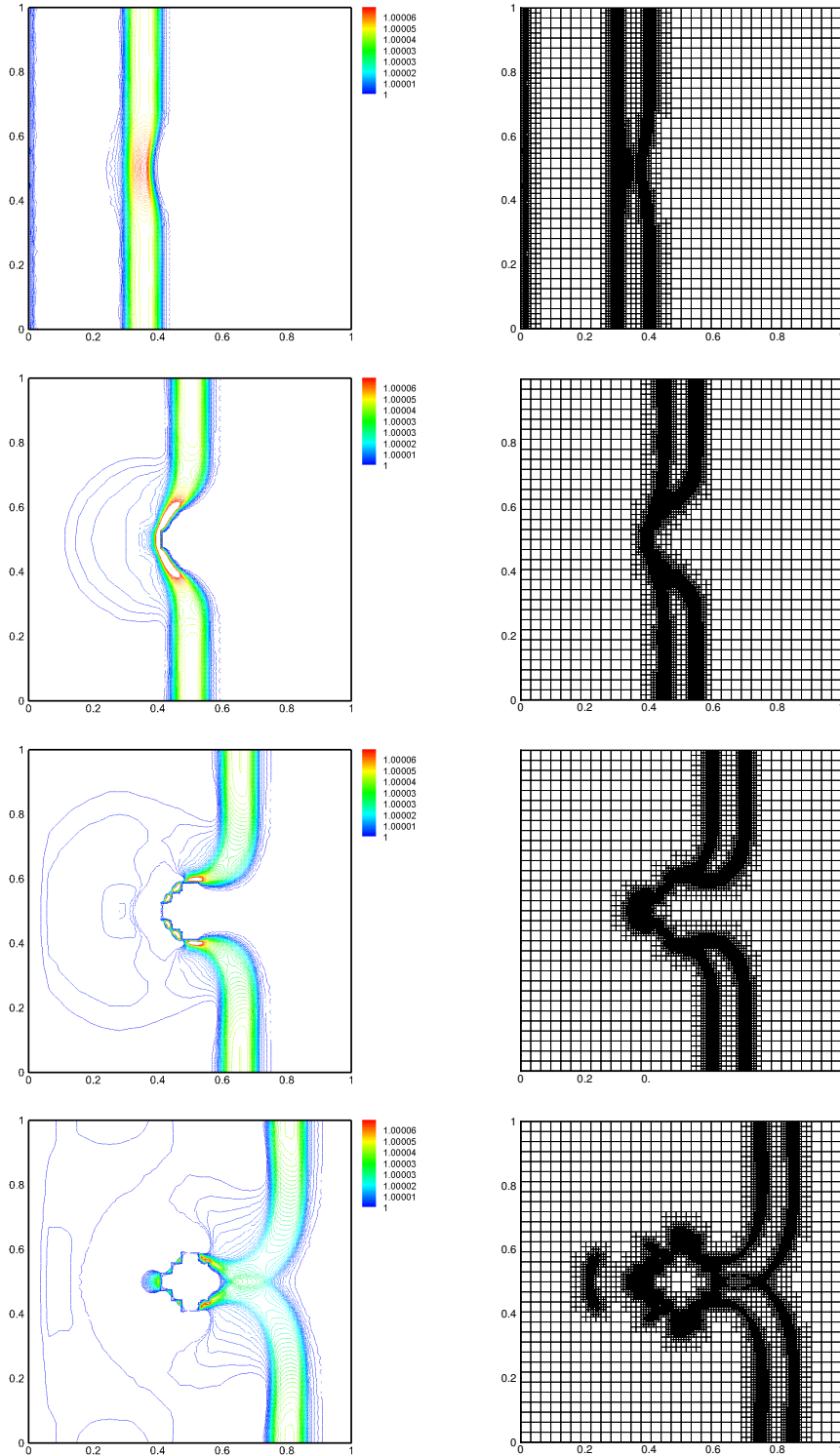


Figure 10: Example 4: Computed water surface $w(x, y, t)$ (left column) and the corresponding quadtree grids (right column) for $t = 0.2, 0.35, 0.5,$ and 0.65 (from top to down) obtained using the well-balanced central-upwind quadtree scheme.

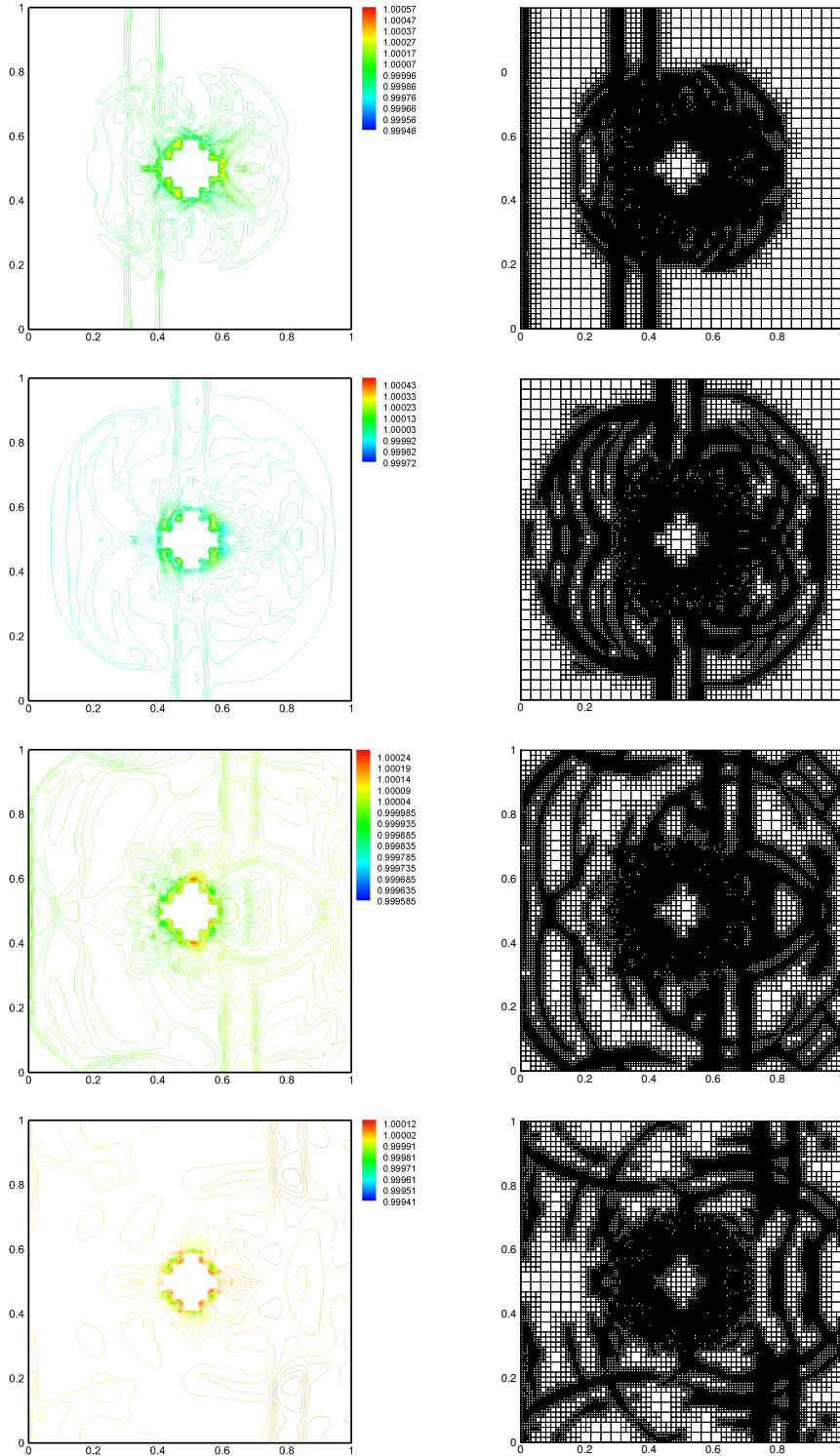


Figure 11: Same as Figure 10, but for the non-well-balanced central-upwind quadtree scheme.

C_{seed} would have increased the computational cost as the local gradients are relatively large in most parts of the computational domain.

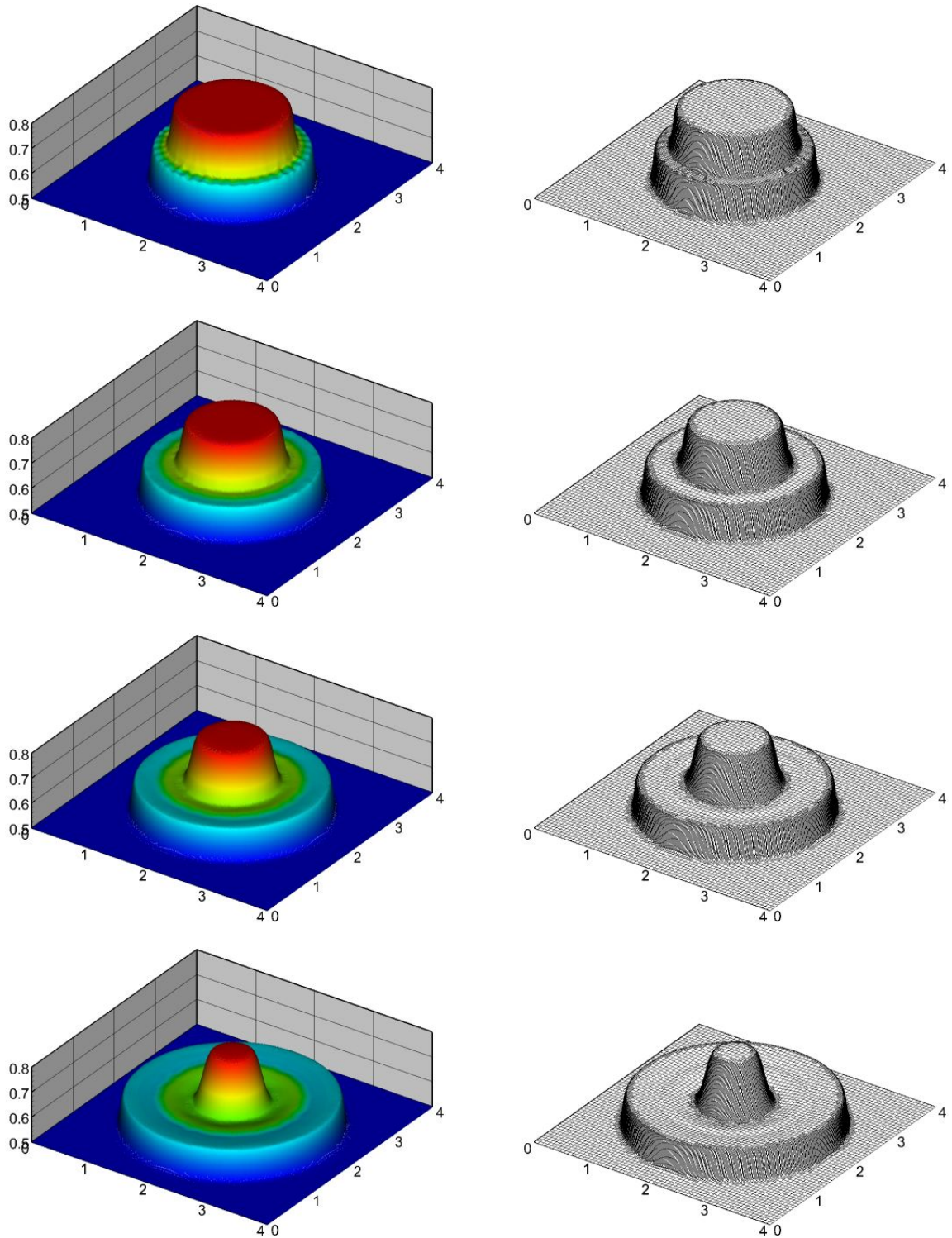


Figure 12: Example 5: Computed water surface $w(x, y, t)$ (left column) and the corresponding quadtree grids (right column) for $t = 0.05, 0.1, 0.15,$ and 0.2 (from top to down).

We compute the solution twice: first, we use the flat bottom topography $B(x, y) \equiv 0$ in order to demonstrate the ability of the scheme to capture hydraulic jumps and sharp waves, and second, we use the bottom topography given by

$$B(x, y) = 0.95 \left[e^{-10(x-1.9)^2-50(y-0.7)^2} + e^{-20(x-2.2)^2-50(y-0.3)^2} \right]$$

and shown in Figure 13 together with the initial quadtree grid for $m = 9$ (notice that the grid is refined near the boundaries at the contraction to improve accuracy). In the nonflat bottom topography case, the water at the top of the humps is quite shallow (that is why this is a good example to test the positivity preserving property) and the Froude number there is initially about 2.

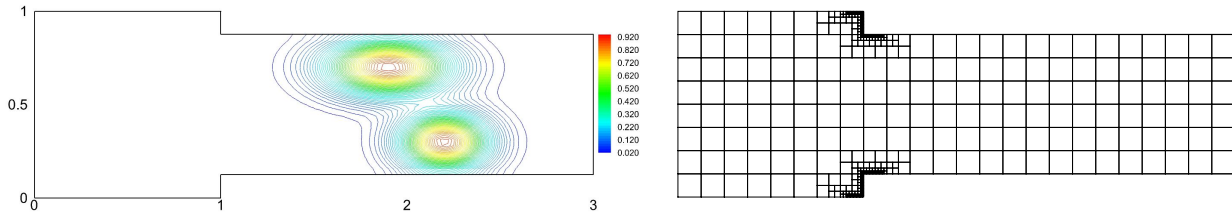


Figure 13: Example 6: Bottom topography (left) and initial quadtree grid with $m = 9$ (right).

We compute the solution until the final time $t = 2$ in order to simulate a transient flow state. We plot the snapshots of w at times $t = 0.5, 1, 1.5$ and 2 in Figures 14 and 15 for the flat and nonflat bottom topographies, respectively. As one can see, the proposed central-upwind quadtree scheme preserves positivity of the computed water depth and is able to capture hydraulic jumps. Increasing m from 8 to 9 clearly improves the accuracy and resolution of the hydraulic jumps. Finally, in Table 1, we present the minimum and maximum number of cells during the time evolution for different quadtree levels and topographies.

Table 2: Example 6: Minimum and maximum number of cells for each of the four solutions.

Quadtree level	$m = 8$		$m = 9$	
	min	max	min	max
$B(x, y) \equiv 0$	298	3154	436	10954
$B(x, y) \neq 0$	298	5140	436	21340

5. Conclusion

An adaptive, well-balanced, positivity preserving central-upwind scheme over quadtree grids for the shallow water equations over irregular bottom topography has been presented. Six numerical experiments have been performed in order to verify the accuracy and robustness of the proposed scheme. The first numerical benchmark test has addressed the accuracy of the scheme. The second numerical example has focused on the positivity and symmetry preserving as well as adaptability of the scheme. The third and fourth numerical examples have demonstrated the

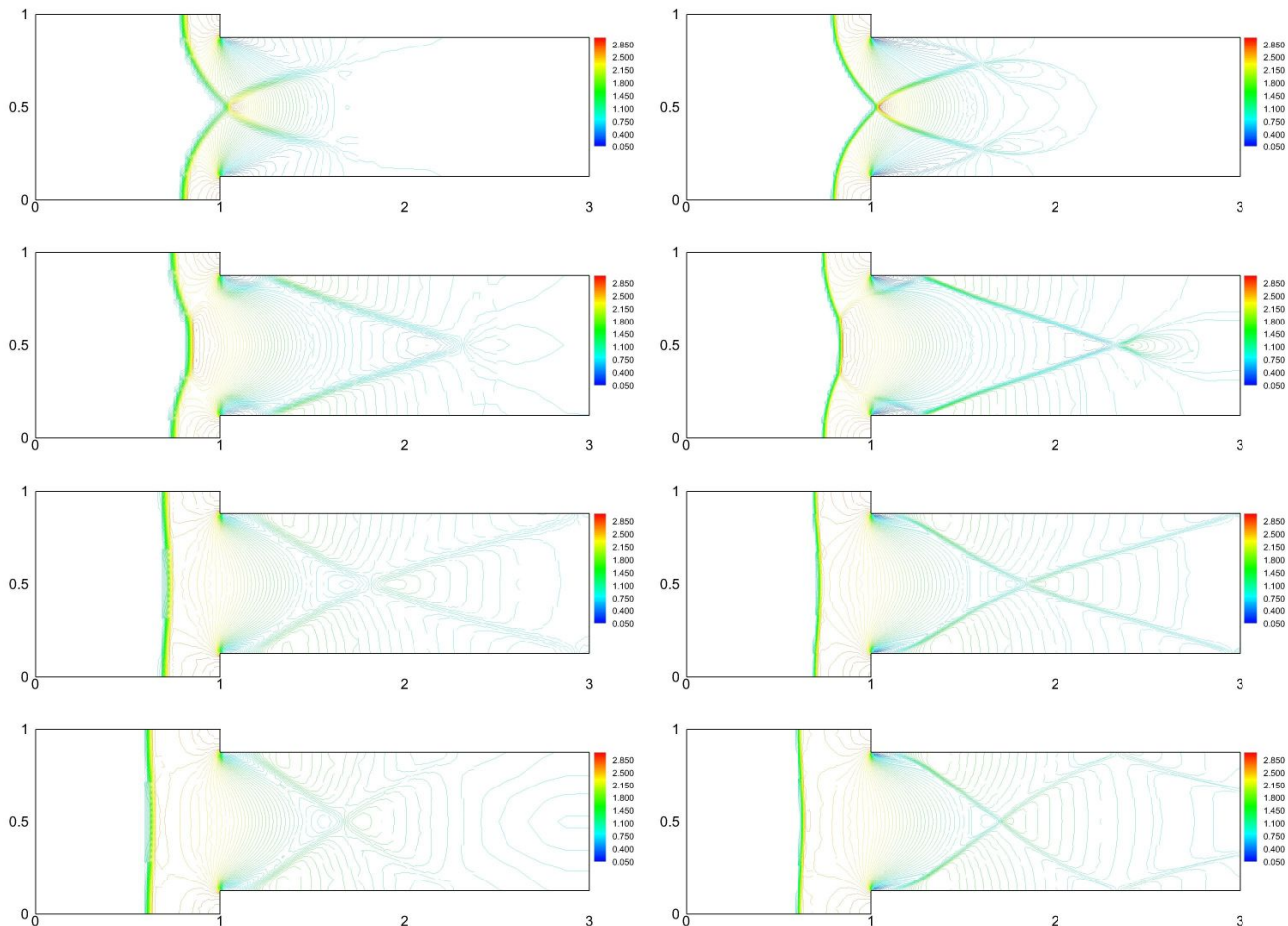


Figure 14: Example 6: Computed water surface $w(x, y, t)$ for $t = 0.5, 1, 1.5$ and 2 (from top to down) obtained using the flat bottom topography for $m = 8$ (left column) and $m = 9$ (right column).

well-balanced property, symmetry preserving and adaptability features of the proposed method. The fifth test has focused on the capability of the scheme to model flows over a discontinuous bottom topography. The last numerical example has demonstrated the positivity preserving and shock-capturing features of the method. The obtained results show that the proposed central-upwind quadtree scheme can improve the performance and efficiency of calculations compared with regular Cartesian grids.

Acknowledgment: The work of A. Kurganov was supported in part by NSFC grant 11771201 and by the fund of the Guangdong Provincial Key Laboratory of Computational Science and Material Design (No. 2019B030301001).

References

- [1] K. Aizawa, K. Motomura, S. Kimura, R. Kadowaki, J. Fan, Constant time neighbor finding in quadtrees: An experimental result, in: 3rd International Symposium on Communications, Control and Signal Processing, 2008. ISCCSP 2008., IEEE, 505–510, 2008.

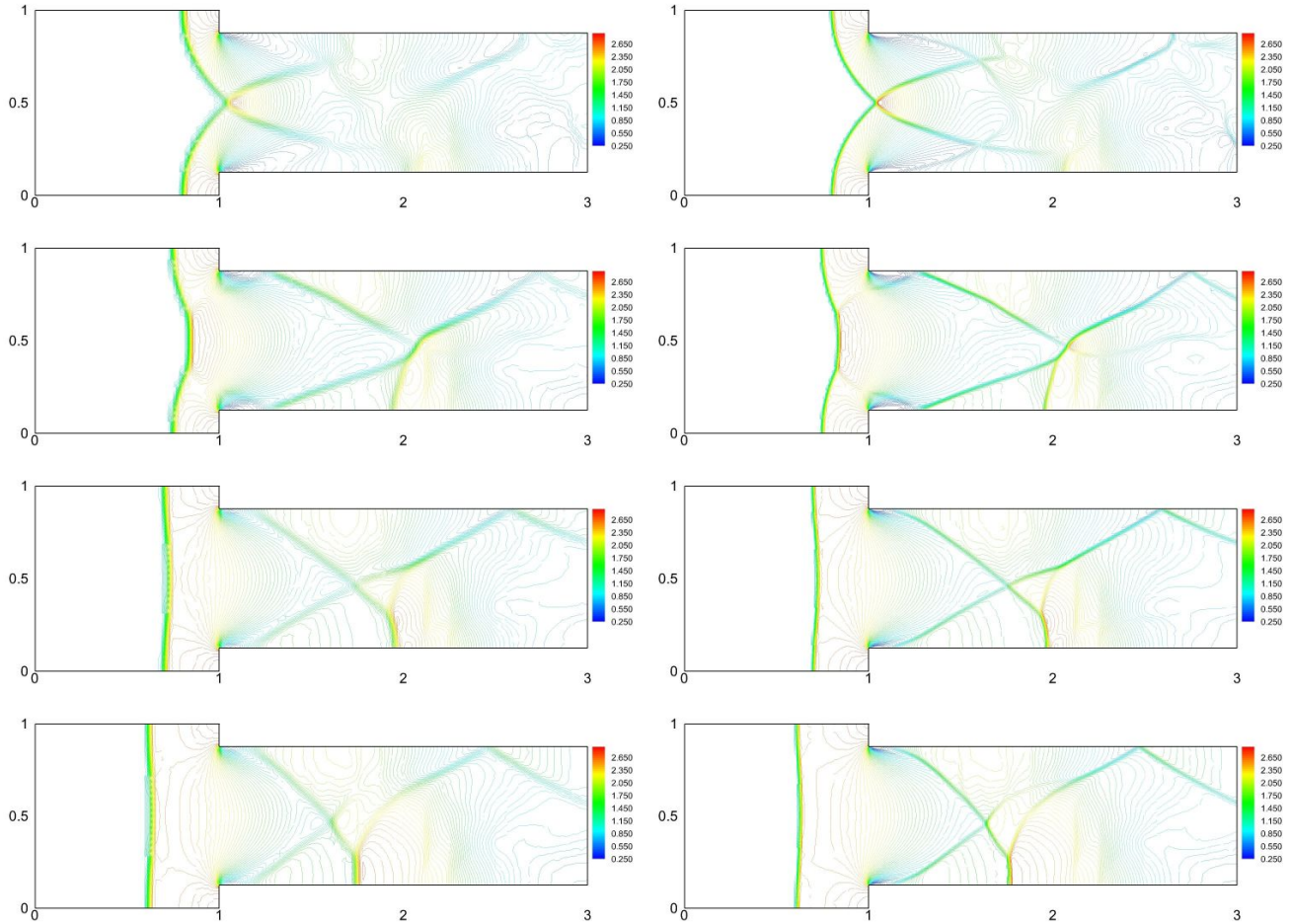


Figure 15: Same as Figure 14, but for the nonflat bottom topography.

- [2] H. An, S. Yu, Well-balanced shallow water flow simulation on quadtree cut cell grids, *Adv. Water Resour.* 39 (2012) 60–70.
- [3] E. Audusse, F. Bouchut, M.-O. Bristeau, R. Klein, B. Perthame, A fast and stable well-balanced scheme with hydrostatic reconstruction for shallow water flows, *SIAM J. Sci. Comput.* 25 (2004) 2050–2065.
- [4] E. Audusse, M.-O. Bristeau, A well-balanced positivity preserving “second-order” scheme for shallow water flows on unstructured meshes, *J. Comput. Phys.* 206 (1) (2005) 311–333.
- [5] A. Beljadid, A. Mohammadian, A. Kurganov, Well-balanced positivity preserving cell-vertex central-upwind scheme for shallow water flows, *Comput. & Fluids* 136 (2016) 193–206.
- [6] M. Berger, M. Aftosmis, S. Muman, Analysis of slope limiters on irregular grids, in: *43rd AIAA Aerospace Sciences Meeting and Exhibit*, 1–22, 2005.
- [7] M. Bern, D. Eppstein, S.-H. Teng, Parallel construction of quadtrees and quality triangulations, *Internat. J. Comput. Geom. Appl.* 9 (6) (1999) 517–532.

- [8] C. Berthon, F. Marche, A positive preserving high order VFRoe scheme for shallow water equations: a class of relaxation schemes, *SIAM J. Sci. Comput.* 30 (5) (2008) 2587–2612.
- [9] A. Bollermann, G. Chen, A. Kurganov, S. Noelle, A well-balanced reconstruction of wet/dry fronts for the shallow water equations, *J. Sci. Comput.* 56 (2) (2013) 267–290.
- [10] A. Bollermann, S. Noelle, M. Lukáčová-Medviděová, Finite volume evolution Galerkin methods for the shallow water equations with dry beds, *Commun. Comput. Phys.* 10 (2) (2011) 371–404.
- [11] A. G. L. Borthwick, S. Cruz Leon, J. Jozsa, Adaptive quadtree model of shallow-flow hydrodynamics, *Journal of Hydraulic Research* 39 (4) (2001) 413–424, ISSN 0022-1686.
- [12] A. G. L. Borthwick, R. D. Marchant, G. J. M. Copeland, Adaptive hierarchical grid model of water-borne pollutant dispersion, *Adv. Water Resour.* 23 (8) (2000) 849–865.
- [13] S. Bryson, Y. Epshteyn, A. Kurganov, G. Petrova, Well-balanced positivity preserving central-upwind scheme on triangular grids for the Saint-Venant system, *M2AN Math. Model. Numer. Anal.* 45 (3) (2011) 423–446.
- [14] S. Bryson, D. Levy, Balanced central schemes for the shallow water equations on unstructured grids, *SIAM J. Sci. Comput.* 27 (2005) 532–552.
- [15] A. J. C. de Saint-Venant, Théorie du mouvement non-permanent des eaux, avec application aux crues des rivières et à l’introduction des marées dans leur lit., *C.R. Acad. Sci. Paris* 73 (1871) 147–154, 237–240.
- [16] M. Dumbser, V. Casulli, A staggered semi-implicit spectral discontinuous Galerkin scheme for the shallow water equations, *Applied Mathematics and Computation* 219 (15) (2013) 8057 – 8077.
- [17] J. M. Gallardo, C. Parés, M. Castro, On a well-balanced high-order finite volume scheme for shallow water equations with topography and dry areas, *J. Comput. Phys.* 227 (1) (2007) 574–601.
- [18] S. Gottlieb, D. Ketcheson, C.-W. Shu, *Strong stability preserving Runge-Kutta and multi-step time discretizations*, World Scientific Publishing Co. Pte. Ltd., Hackensack, NJ, 2011.
- [19] S. Gottlieb, C.-W. Shu, E. Tadmor, *Strong stability-preserving high-order time discretization methods*, *SIAM Rev.* 43 (1) (2001) 89–112.
- [20] D. M. Greaves, A. G. L. Borthwick, On the use of adaptive hierarchical meshes for numerical simulation of separated flows, *Internat. J. Numer. Methods Fluids* 26 (3) (1998) 303–322.
- [21] M. E. Hubbard, On the accuracy of one-dimensional models of steady converging/diverging open channel flows, *Internat. J. Numer. Methods Fluids* 35 (2001) 785–808.
- [22] G. Kesserwani, Q. Liang, Dynamically adaptive grid based discontinuous Galerkin shallow water model, *Advances in Water Resources* 37 (2012) 23–39, ISSN 0309-1708.

- [23] A. Kurganov, Finite-volume schemes for shallow-water equations, *Acta Numer.* 27 (2018) 289–351.
- [24] A. Kurganov, D. Levy, Central-upwind schemes for the Saint-Venant system, *M2AN Math. Model. Numer. Anal.* 36 (3) (2002) 397–425.
- [25] A. Kurganov, C.-T. Lin, On the reduction of numerical dissipation in central-upwind schemes, *Commun. Comput. Phys.* 2 (1) (2007) 141–163.
- [26] A. Kurganov, S. Noelle, G. Petrova, Semidiscrete central-upwind schemes for hyperbolic conservation laws and Hamilton-Jacobi equations, *SIAM J. Sci. Comput.* 23 (3) (2001) 707–740.
- [27] A. Kurganov, G. Petrova, A second-order well-balanced positivity preserving central-upwind scheme for the Saint-Venant system, *Commun. Math. Sci.* 5 (1) (2007) 133–160.
- [28] A. Kurganov, M. Prugger, T. Wu, Second-order fully discrete central-upwind scheme for two-dimensional hyperbolic systems of conservation laws, *SIAM J. Sci. Comput.* 39 (3) (2017) A947–A965.
- [29] A. Kurganov, E. Tadmor, New high-resolution central schemes for nonlinear conservation laws and convection-diffusion equations, *J. Comput. Phys.* 160 (1) (2000) 241–282.
- [30] A. Kurganov, E. Tadmor, Solution of two-dimensional Riemann problems for gas dynamics without Riemann problem solvers, *Numer. Methods Partial Differential Equations* 18 (2002) 584–608.
- [31] D. Kuzmin, On the design of general-purpose flux limiters for finite element schemes. I. Scalar convection, *J. Comput. Phys.* 219 (2) (2006) 513–531.
- [32] W.-K. Lee, A. G. L. Borthwick, P. H. Taylor, A fast adaptive quadtree scheme for a two-layer shallow water model, *J. Comput. Phys.* 230 (12) (2011) 4848–4870.
- [33] R. J. LeVeque, Balancing source terms and flux gradients in high-resolution Godunov methods: the quasi-steady wave-propagation algorithm, *J. Comput. Phys.* 146 (1) (1998) 346–365.
- [34] Q. Liang, A. G. Borthwick, Adaptive quadtree simulation of shallow flows with wetdry fronts over complex topography, *Computers & Fluids* 38 (2) (2009) 221–234, ISSN 00457930.
- [35] Q. Liang, A. G. L. Borthwick, G. Stelling, Simulation of dam- and dyke-break hydrodynamics on dynamically adaptive quadtree grids, *International Journal for Numerical Methods in Fluids* 46 (September) (2004) 127–162, doi:10.1002/fld.748.
- [36] Q. Liang, J. Hou, X. Xia, Contradiction between the C-property and mass conservation in adaptive grid based shallow flow models : cause and solution, *International Journal for Numerical Methods in Fluids* 78 (February) (2015) 17–36.
- [37] G.-F. Lin, J.-S. Lai, W.-D. Guo, Finite-volume component-wise TVD schemes for 2D shallow water equations, *Adv. Water Resour.* 26 (8) (2003) 861–873.

- [38] X. Liu, J. Albright, Y. Epshteyn, A. Kurganov, Well-balanced positivity preserving central-upwind scheme with a novel wet/dry reconstruction on triangular grids for the Saint-Venant system, *J. Comput. Phys.* 374 (2018) 213–236.
- [39] X. Liu, A. Mohammadian, A. Kurganov, J. A. Infante Sedano, Well-balanced central-upwind scheme for a fully coupled shallow water system modeling flows over erodible bed, *J. Comput. Phys.* 300 (2015) 202–218.
- [40] V. Michel-dansac, C. Berthon, S. Clain, A well-balanced scheme for the shallow-water equations with topography, *Computers and Mathematics with Applications* 72 (3) (2016) 568–593, ISSN 0898-1221.
- [41] D. Moore, The cost of balancing generalized quadtrees, in: *Proceedings of the third ACM symposium on Solid modeling and applications*, ACM Press, New York, New York, USA, 305–312, 1995.
- [42] F. Pascal, J. L. Marechal, Fast adaptive quadtree mesh generation, in: *7th International Meshing Roundtable*, Citeseer, 211–224, 1998.
- [43] S. Popinet, Gerris: a tree-based adaptive solver for the incompressible Euler equations in complex geometries, *J. Comput. Phys.* 190 (2) (2003) 572–600.
- [44] S. Popinet, R. M. Gorman, G. J. Rickard, H. L. Tolman, A quadtree-adaptive spectral wave model, *Ocean Model.* 34 (1-2) (2010) 36–49.
- [45] M. Ricchiuto, An explicit residual based approach for shallow water flows, *J. Comput. Phys.* 280 (2015) 306–344.
- [46] M. Rodriguez-Paz, J. Bonet, A corrected smooth particle hydrodynamics formulation of the shallow-water equations, *Comput. & Structures* 83 (17-18) (2005) 1396–1410.
- [47] B. Rogers, M. Fujihara, A. G. L. Borthwick, Adaptive Q-tree Godunov-type scheme for shallow water equations, *Internat. J. Numer. Methods Fluids* 35 (3) (2001) 247–280.
- [48] H. Samet, Neighbor finding techniques for images represented by quadtrees, *Comput. Vision Graph.* 18 (1) (1982) 37–57.
- [49] H. Samet, Algorithms for the conversion of quadtrees to rasters, *Comput. Vision Graph.* 26 (1) (1984) 1–16.
- [50] H. Samet, The quadtree and related hierarchical data structures, *Comput. Surveys* 16 (2) (1984) 187–260.
- [51] H. Samet, *Foundations of Multidimensional and Metric Data Structures*, Morgan Kaufmann, first edn., 2006.
- [52] H. Samet, C. A. Shaffer, A model for the analysis of neighbor finding in pointer-based quadtrees, *IEEE T. Pattern Anal.* PAMI-7 (6) (1985) 717–720.

- [53] J. Sankaranarayanan, H. Samet, A. Varshney, A fast all nearest neighbor algorithm for applications involving large point-clouds, *Comput. Graph.* 31 (2) (2007) 157–174.
- [54] H. Shirkhani, A. Mohammadian, O. Seidou, A. Kurganov, A well-balanced positivity-preserving central-upwind scheme for shallow water equations on unstructured quadrilateral grids, *Comput. & Fluids* 126 (2016) 25–40.
- [55] P. K. Sweby, High resolution schemes using flux limiters for hyperbolic conservation laws, *SIAM J. Numer. Anal.* 21 (5) (1984) 995–1011.
- [56] P. M. Vaidya, An $O(n \log n)$ algorithm for the all-nearest-neighbors problem, *Discrete Comput. Geom.* 4 (2) (1989) 101–115.
- [57] K. F. C. Yiu, D. M. Greaves, S. Cruz, A. Saalehi, A. G. L. Borthwick, Quadtree grid generation: Information handling, boundary fitting and CFD applications, *Comput. & Fluids* 25 (8) (1996) 759–769.